Receptor tyrosine kinases CAD96CA and FGFR1 function as the cell membrane receptors of insect juvenile hormone

Yan-Xue Li[1], Xin-Le Kang[1], Yan-Li Li[1], Xiao-Pei Wang[1], Qiao Yan[1], Jin-Xing Wang[1] and Xiao-Fan Zhao[1]*

[1] Shandong Provincial Key Laboratory of Animal Cells and Developmental Biology, School of Life Sciences, Shandong University, China

*Corresponding author: Xiao-Fan Zhao

Email: xfzhao@sdu.edu.cn

Abstract

Juvenile hormone (JH) is important to maintain insect larval status; however, its cell membrane receptor has not been identified. Using the lepidopteran insect *Helicoverpa armigera* (cotton bollworm), a serious agricultural pest, as a model, we determined that receptor tyrosine kinases (RTKs) cadherin 96ca (CAD96CA) and fibroblast growth factor receptor homologue (FGFR1) function as JH cell membrane receptors by their roles in JH-regulated gene expression, larval status maintaining, calcium increase, phosphorylation of JH intracellular receptor MET1 and cofactor Taiman, and high affinity to JH III. Gene knockout of *Cad96ca* and *Fgfr1* by CRISPR/Cas9 in embryo and knockdown in various insect cells, and overexpression of CAD96CA and FGFR1 in mammalian HEK-293T cells all supported CAD96CA and FGFR1 transmitting JH signal as JH cell membrane receptors.

Keywords: receptor tyrosine kinase, juvenile hormone, cell membrane receptor, methoprene tolerant protein 1, Taiman

Introduction

Juvenile hormone (JH) plays a vital role in insect development and maintaining insect larval status. JH is an acyclic sesquiterpenoid known to enter cells freely via diffusion because of its lipid-soluble character (*Riddiford, 2020*). JH binds its intracellular receptor methoprene-tolerant protein (MET), a basic helix-loop-helix/Per-ARNT-SIM (bHLH-PAS) family protein (*Charles et al., 2011; Jindra et al., 2021*). MET forms a transcription complex with the transcription factor Taiman (TAI, also known as FISC, p160/SRC, and is a steroid receptor coactivator) to initiate gene transcription *(Charles et al., 2011; Zhu et al., 2003*). An important gene in the JH pathway is Krüppel homologue 1 (Kr-h1), which encodes the zinc-finger transcription factor Kr-h1 (*Minakuchi et al., 2008; Pecasse et al., 2000; Wu et al., 2021*). Kr-h1 acts downstream of MET and is induced rapidly by JH to regulate larval growth and development (*Minakuchi et al., 2009*). Other genes, for example, the early trypsin gene of *Aedes aegypti* (*AaEt*) (*Li et al., 2011; Noriega et al., 2003*), JH-inducible 21 kDa protein (*Jhp21*) (*Zhang et al., 1996*), JH esterase (*Jhe*) (*Feng et al., 1999; Wroblewski et al., 1990*), vitellogenin (*Vg*) (*Comas et al., 1999; Xu et al., 2014*), *Drosophila* JH-inducible gene 1(*Jhi-1*), and JH-inducible gene 26 (*Jhi-26*) *(Dubrovsky et al., 2000*) are regulated by JH.

However, some studies suggest that cell membrane receptors also play essential roles in JH signaling (*Davey, 2000; Jindra et al., 2021*). For example, in *A*. *aegypti*, receptor tyrosine kinases (RTKs) are involved in JH-induced rapid increases in inositol 1,4,5-trisphosphate, diacylglycerol, and intracellular calcium, leading to activation of calcium/calmodulin-dependent protein kinase II (CaMKII) to phosphorylation of MET and Tai, resulting in *Kr-h1* gene transcription in response to JH (*Liu et al., 2015*). JH III, also via RTKs, leads to rapid calcium release and influx in *Helicoverpa armigera* epidermal cells (HaEpi cells) (*Wang et al., 2016*). JH induces MET1 phosphorylation, increasing MET interaction with TAI, which enhances Kr-h1 transcription in *H. armigera (Li et al., 2021*). In *Drosophila melanogaster*, JH through RTK and PKC protein kinase C (PKC) induces phosphorylation of ultraspiracle (USP) (*Gao et al., 2022*). The phenomenon that RTK transmits JH signal has long been predicted *(Liu et al., 2015; Ojani et al., 2016*); however, the RTKs critical for JH signaling have yet to be identified from numerous RTKs *in vivo*.

RTKs constitute a class of cell surface transmembrane proteins that play important roles in mediating extracellular to intracellular signaling. Humans carry approximately 60 RTKs *(Manning et al., 2002*), the *Drosophila* genome encodes 21 RTK genes (*Sopko and Perrimon, 2013*), *Bombyx mori* has 20 RTKs (*Alexandratos et al., 2016*), and the *German cockroach* genome identified 16 RTKs (*Li et al., 2022*). *H. armigera* has 20 RTK candidates with gene codes in the *H. armigera* genome by our analysis. The cotton bollworm, is a well-known and worldwide distributing agricultural pest in Lepidoptera, which threatens cotton and many other vegetable crops by rapidly producing resistance to various chemical insecticides and Bt-transgenic cotton. Using *H. armigera* as a model, we focus on identifying the RTKs functioning as the JH receptors and demonstrating the mechanism. We screened 20 RTKs in the *H. armigera* genome and determined that cadherin 96ca (CAD96CA) and fibroblast growth factor receptor 1 (FGFR1) have high affinity to JH III and function as JH cell membrane receptors. These data not only improve our knowledge of JH signaling and open the door to studying insect development, but also present new targets to explore the new growth regulators to control the pest.

Results

The screen of the RTKs involved in JH signaling

To explore which RTKs may be involved in JH signaling, the total of RTKs were identified in the *H. armigera* genome. We found 20 RTK-like proteins encoded in the *H. armigera* genome and named the RTKs according to the nomenclature typically used in the genome or according to their homologues in *B. mori* or *D. melanogaster* (*Supplementary file 1*). Phylogenetic analysis showed that the 20 RTK candidates in *H. armigera* were conserved in *B. mori* and *D. melanogaster* (*Figure 1—figure supplement 1*). All the analyzed RTKs were grouped according to the basis of their structural characteristics and homology to the structure of 20 subfamilies of

human (*Honegger et al., 1989; Lemmon and Schlessinger, 2010; Sparrow et al., 1997; Yarden and Ullrich, 1988*); the cell wall integrity and stress response component kinase (WSCK), tyrosine-protein kinase receptor torso like (TORSO) and serine/threonine-protein kinase STE20-like (STE 20-like) were not classed (*Figure 1—figure supplement 2*).

To identify the RTKs involved in JH III signaling, 20 RTKs of *H. armigera* were knocked down by RNA interference (RNAi) in HaEpi cells using JH III-induced *Kr-h1*, *Vg*, *Jhi-1*, and *Jhi-26* gene expression as readouts. When *Cad96ca*, *Drl* (encoding derailed), *Fgfr1*, *Nrk* (encoding neurotropic receptor kinase), *Vegfr1* (encoding vascular endothelial growth factor receptor 1), and *Wsck* were knocked down, respectively, JH III-upregulated expression of *Kr-h1* was decreased. However, knocking down other *Rtks* did not decrease the *Kr-h1* transcription level. When *Cad96ca*, *Drl*, *Fgfr1*, *Nrk*, *Vegfr1*, *Wsck*, and *Inr* (encoding insulin-like receptor) were knocked down, JH III-upregulated expression of *Vg* was decreased. RNAi of RTKs did not affect JH-induced *Jhi-1* expression. When *Cad96ca*, *Fgfr1*, *Nrk*, and *Vegfr1* were knocked down, JH III-upregulated expression of *Jhi-26* was decreased (*Figure 1A*). *Rtks* were confirmed to be knocked down significantly in HaEpi cells (*Figure 1—figure supplement 3A*). Off–target effects of their knockdown were excluded in genes we detected. Off–target genes were selected based on the identity rate of nucleotide sequences (*Figure 1—figure supplement 3B*). By the primary screening of RNAi, six RTKs, CAD96CA, DRL, FGFR1, NRK, VEGFR1, and WSCK were chosen for further screening.

The tissue–specific and developmental expression profiles of the six selected RTKs were determined using qRT–PCR to identify their possible roles in tissues at different developmental stages. The mRNA levels of *Vegfr1*, *Drl*, *Cad96ca*, and *Nrk* showed no expression specificity in the epidermis, midgut, or fat body. Their transcript levels were high at the sixth instar feeding stage (6th–6 h to 6th–48 h) compared with those at the metamorphic molting stage (6th–72 h to 6th–120 h) and pupal stages (P–0 d to P–8 d). *Fgfr1* was highly expressed in the midgut at these feeding stages. *Wsck* was highly expressed from the 6th–48 h to the pupal stage and showed no tissue specificity (*Figure 1—figure supplement 4A*). These data suggested that most of the RTKs are distributed in various tissues and highly expressed during larval feeding stages.

We further examined the roles played by these six RTKs in JH III-delayed pupation by injecting double-stranded RNA (dsRNA) into the fifth instar 20 h larval haemocoel. Interference of these six RTK genes in larvae led to the expression of *Kr-h1* decreasing significantly. When *Cad96ca*, *Nrk*, *Fgfr1*, and *Wsck* were knocked down, the expression of *Br-z7* (encoding broad isoform Z7) was increased (*Figure 1—figure supplement 4B*). The pupation time was approximately 162 h in 93% of the larvae in the dimethyl sulfoxide (DMSO) control group. After injection of JH III, the pupation time was approximately 187 h in 76% of the larvae, which was 25 h later than that of the DMSO control group, suggesting that JH III delayed pupation. In the *dsGFP*+JH III-injected control, larvae pupated at approximately the same time as larvae after JH III treatment. In the *dsVegfr1*+JH III and *dsDrl*+JH III treatment groups, most larvae exhibited delayed pupation; only 9–10% of the larvae did not show delayed pupation, and 28–30% died at the larval or pupal stage. However, 66–68% of the larvae did not show delayed pupation after *dsCad96ca*+JH III, *dsNrk*+JH III, *dsFgfr1*+JH III or *dsWsck*+JH III injection (*Figure 1B, C and Figure 1—figure supplement 4C*). These results indicated that VEGFR1 and DRL are essential for survival and that CAD96CA, NRK, FGFR1, and WSCK are involved in JH III-induced delayed pupation.

To address the mechanism involved in the RTK effects on JH signaling, we examined the roles played by the selected RTKs in JH III-induced cellular responses by knocking down RTK gene expression in HaEpi cells. JH III-induced rapid calcium mobilization was repressed after knockdown of *Vegfr1*, *Drl*, *Cad96ca*, *Nrk*, *Fgfr1* or *Wsck* compared with that after *dsGFP* knockdown (*Figure 2A*). The efficacy of RNAi was confirmed (*Figure 2B*). However, only *Cad96ca*, *Nrk* or *Fgfr1* knocking down decreased the JH III-induced phosphorylation of MET1 and TAI (*Figure 2C*). The results suggested that these aforementioned RTKs are all involved in JH III-induced rapid cellular calcium increase but are differentially involved in JH III-induced MET1 and TAI phosphorylation.

CAD96CA and FGFR1 had high affinity to JH III

The affinity of CAD96CA, FGFR1, NRK, and OTK for JH III was determined using saturable specific–binding curve analysis via microscale thermophoresis (MST). The experiment used full–length sequences of CAD96CA, FGFR, NRK, and OTK. CAD96CA-CopGFP-His, FGFR1-CopGFP-His, NRK-CopGFP-His, and OTK-CopGFP-His were overexpressed in the Sf9 cell line (Sf9 cells expressed the proteins at a higher level than HaEpi cells) and then, the proteins were isolated separately to determine the JH III-binding strength of each. Immunocytochemistry showed that CAD96CA-CopGFP-His, FGFR1-CopGFP-His, NRK-CopGFP-His, and OTK-CopGFP-His located in the plasma membrane (*Figure 3A*). The purity of the proteins was assessed and confirmed using sodium dodecyl sulfate–polyacrylamide gel electrophoresis (SDS–PAGE) with Coomassie brilliant blue staining (*Figure 3B*). CAD96CA-CopGFP-His binding to JH III exhibited a dissociation constant (Kd) = 11.96 ± 1.61 nM. Similarly, the saturable specific binding of FGFR1-CopGFP-His to JH III exhibited a Kd = 23.61 ± 0.90 nM, and NRK-CopGFP-His and OTK-CopGFP-His showed no obvious binding (*Figure 3C*). These results suggested that CAD96CA and FGFR1 bind JH III.

The JH intracellular receptor MET has been reported to bind to JH in *Tribolium* (*Charles et al., 2011*); therefore, the JH intracellular receptor MET1 in *H. armigera* was used as the positive control in analyses to assess the applicability of the MST method. MET1-CopGFP-His and CopGFP-His were overexpressed in the Sf9 cell line and then isolated to determine the strength of their binding to JH III. Immunocytochemistry showed the nuclear location of MET1 (*Figure 3—figure supplement 1A*). The purities of the isolated CopGFP-His and MET1-CopGFP-His proteins were examined and confirmed using SDS–PAGE with coomassie brilliant blue staining (*Figure 3—figure supplement 1B*). The saturable specific binding of MET1-CopGFP-His to JH III exhibited a Kd = 6.38 ± 1.41 nM. CopGFP-His showed weaker binding to JH III (*Figure 3—figure supplement 1C*). In comparison with the Kd of *Tribolium* MET to JH III of 2.94 ± 0.68 nM as detected by [^{3}H]JH III (*Charles et al., 2011*), the Kd of MET1 binding to JH III was determined to validate that the MST method was a valid approach to detect the JH III binding activity of a protein.

To validate CAD96CA and FGFR1 binding JH III, saturation assays were performed using the analogs of JH, the farnesol, methoprene and farnesoate (MF). Results showed that CAD96CA-CopGFP-His bound farnesol with a Kd of 1039.2 ± 0.68 nM. CAD96CA-CopGFP-His bound methoprene with a Kd of 553.94 ± 1.11 nM. CAD96CA-CopGFP-His bound methyl farnesoate (MF) with a Kd of 446.55 ± 0.80 nM. CAD96CA-CopGFP-His bound JH III with a Kd of 12.10 ± 1.4 nM (*Figure 3D*). The results confirmed that CAD96CA has the highest affinity to JH III.

Because methoprene is known as an effective juvenoid (*Konopova and Jindra, 2007*) and competes with JH III in binding to MET (*Charles et al., 2011*), therefore, the compete experiment was performed to confirm CAD96CA bound both JH III. CAD96CA-CopGFP-His bound to methoprene plus JH III with a Kd value of 261.43 ± 0.81 nM, whereas, CAD96CA-CopGFP-His bound to methoprene with a Kd value of 563.49 ± 0.7 (*Figure 3E*). These suggested that CAD96CA-CopGFP-His has the highest affinity to JH III compared with the analogs.

Similarly, the saturable specific binding of FGFR1-CopGFP-His bound farnesol with a Kd = 23810 ± 0.51 nM; FGFR1-CopGFP-His bound methoprene with a Kd = 529.68 ± 0.60 nM; FGFR1-CopGFP-His to MF exhibited a Kd = 417.20 ± 0.66 nM; and FGFR1-CopGFP-His to JH III exhibited a Kd = 21.45 ± 1.02 (*Figure 3F*), suggesting FGFR1 had the highest affinity to JH III. The compete binding of FGFR1-CopGFP-His to methoprene plus JH III with a Kd value = 349.27 ± 0.58 nM, whereas, FGFR1-CopGFP-His to methoprene with a Kd value = 523.57 ± 0.89 (*Figure 3G*). These suggested that FGFR1 has the highest affinity to JH III compared with the analogs.

Various mutants of CAD96CA and FGFR1 were further constructed to identify the key motifs in CAD96CA and FGFR1 critical for JH binding. Truncated mutations were performed on extracellular regions of CAD96CA and FGFR1, including CAD96CA-M1(51-615 AA, amino acid), CAD96CA-M2 (101-615 AA), CAD96CA-M3 (151-615 AA), CAD96CA-M4 (201-615 AA), FGFR1-M1 (101-615 AA), FGFR1-M2 (201-615 AA), FGFR1-M3 (301-615 AA) and FGFR1-M4 (401-615 AA). Mutants were overexpressed, and the encoded mutants located in the plasma membrane,

as confirmed via immunocytochemistry, and the purity of the proteins was confirmed using SDS–PAGE with Coomassie brilliant blue staining (*Figure 3—figure supplement 1D-I*). The affinity of CAD96CA-M2, CAD96CA-M3, and CAD96CA-M4 mutants to JH III was significantly reduced compared with wild-type counterparts (*Figure 3H*). Similarly, the affinity of FGFR1-M2, FGFR1-M3, and FGFR1-M4 mutants to JH III was significantly reduced compared with wild-type counterparts (*Figure 3I*). These results suggested that the extracellular domain 51-151 AA in CAD96CA and the extracellular domain 101-301 AA in FGFR1 play a vital role in JH binding.

The affinity of CAD96CA, FGFR1, NRK, and OTK for JH III was further determined using saturable specific–binding curve analysis via isothermal titration calorimetry (ITC). ITC as an alternative method to further examine the affinity of CAD96CA and FGFR1 to JH III. CAD96CA-CopGFP-His bound JH III with a Kd value of 79.6 ± 27.5 nM. Similarly, the saturable specific binding of FGFR1-CopGFP-His to JH III with a Kd value of 88.5 ± 19.4 nM, and NRK-CopGFP-His and OTK-CopGFP-His showed no remarkable binding (*Figure 3—figure supplement 2*). These results also suggested that CAD96CA and FGFR1 bind JH III.

Gene knockout of *Cad96ca* or *Fgfr1* by CRISPR/Cas9 caused early pupation and a decrease of JH signaling

To verify the roles played by CAD96CA and FGFR1 in JH signaling *in vivo*, we mutated *Cad96ca* or *Fgfr1* by CRISPR/Cas9 technology. We selected two gRNAs targeting different sites in the *Cad96ca* and *Fgfr1* coding regions with a low probability of causing off–target effects. Two gRNAs (referred to as *Cad96ca*-gRNAs) located at the third exon of the *Cad96ca* gene (*Figure 4A*), and two gRNAs (referred to as *Fgfr1*-gRNAs) located at the second exon of the *Fgfr1* gene (*Figure 4B*) were selected for the experiment.

When the Cas9-gRNA injected eggs (105 eggs were injected each for, three injections, a total of 315 experimental eggs) had developed into second instar larvae, the survival rates were determined. The survival rate of the Cas9-gRNA-injected eggs (19.4~20.6%) did not greatly differ from that of the control eggs injected with Dulbecco's phosphate-buffered saline (DPBS) (a survival rate of 22.6%), suggesting that the mixture of gRNA and Cas9 protein was nontoxic to the *H. armigera* eggs. In 61 survivors of Cas9 protein and *Cad96ca*-gRNA injection, 30 mutants were identified by the earlier pupation and sequencing (an editing efficiency of 49.2%). Similarly, in 65 survivors of Cas9 protein and *Fgfr1*-gRNA injection, 35 mutants were identified (an editing efficiency of 53.8%) (*Figure 4C*) by sequencing of the mutants and deducing the mutated amino acid and analyzing off–target (*Figure 4—figure supplement 1*). CRISPR/Cas9 editing by *Cad96ca*-gRNA or *Fgfr1*-gRNA injection resulted in earlier pupation (*Figure 4D*) for about 23~24 h by comparison with normal pupation in 46% and 54% of larvae, respectively, at G0 generation (*Figure 4E*), suggesting that CAD96CA and FGFR1 prevented pupation *in vivo*. The low death rate after *Cad96ca* and *Fgfr1* knockout was because of the chimera of the gene knockout at G0.

To address the mechanism of early pupation caused by knockout of *Cad96ca* or *Fgfr1*, we compared the expression of the genes in the JH and 20E pathways between mutant and wild-type *H. armigera*. Both the mutants *Cad96ca* or *Fgfr1* led to a significant decrease in *Kr-h1* expression and an increase in 20E pathway gene expression compared with the wild-type *H. armigera*, respectively (*Figure 4F and G*), indicating that CAD96CA and FGFR1 prevented pupation by increasing *Kr-h1* expression and repressing 20E pathway gene expression.

To confirm the roles played by CAD96CA and FGFR1 in JH signaling, we further examined the response of HaEpi cells to JH III induction after editing of *Cad96ca* and *Fgfr1* by CRISPR/Cas9 in HaEpi cells using the gRNAs inserted in the pIEx-4-BmU6-gRNA-Cas9-GFP-P2A-Puro plasmid (*Figure 4H*). The mutation of *Cad96ca* and *Fgfr1* in HaEpi cells was confirmed by sequencing the mutants and deduced amino acids (*Figure 4—figure supplement 2A-D*). *Cad96ca* or *Fgfr1* mutation repressed the JH III-induced expression of *Kr-h1* in HaEpi cells compared with wild type cells (*Figure 4I*), and repressed the JH III-induced rapid calcium mobilization in cells (*Figure 4J and Figure 4—figure supplement 2E*), suggesting that CAD96CA and FGFR1 were involved in JH III-induced expression of *Kr-h1* and rapid calcium mobilization. These results supported the hypothesized roles played by CAD96CA and FGFR1 in JH signaling.

CAD96CA and FGFR1 transmitted JH signal in different insect cells and HEK-293T cells

To demonstrate the universality of CAD96CA and FGFR1 in JH signaling in different insect cells, we investigated JH-triggered calcium ion mobilization in Sf9 cells (*S. frugiperda*) and S2 cells (*D. melanogaster*). Knockdown of *Cad96ca* and *Fgfr1* (named *Htl* in *D. melanogaster*), respectively, significantly decreased JH III-induced intracellular Ca^{2+} release and extracellular Ca^{2+} influx (*Figure 5A and B*). The efficacy of RNAi of *Cad96ca* and *Fgfr1* was confirmed in the cells (*Figure 5—figure supplement 1*), suggesting that CAD96CA and FGFR1 had a general function to transmit JH signal in *S. frugiperda* and *D. melanogaster*.

To confirm the roles of CAD96CA and FGFR1 transmitting JH signal, CAD96CA and FGFR1 of *H. armigera* were overexpressed heterogeneously in mammalian HEK-293T cells to exclude the unknown endogenous effect in insect cells. Immunocytochemistry showed that CAD96CA-GFP, FGFR1-GFP, and NRK-GFP located in the plasma membrane. The proteins were confirmed using western blotting (*Figure 5—figure supplement 2A*). HEK-293T cells had no significant changes at calcium ion levels (*Figure 5C*), indicating that HEK-239T cells did not respond to JH III induction. However, when HEK-293T cells were overexpressed CAD96CA and FGFR1, respectively, JH III triggered rapid cytosolic Ca^{2+} increase, by comparison with the DMSO condition, His tag, and other RTK NRK-His controls (*Figure 5D*). These results further confirmed that CAD96CA and FGFR1 transmit JH III signal.

CAD96CA and FGFR1 mutants were used to further confirm their role in transmitting the JH signal. Mutants were overexpressed, and the encoded mutants located in the plasma membrane, as confirmed via immunocytochemistry, and the proteins were confirmed using western blotting (*Figure 5—figure supplement 2B*). Results showed that Ca^{2+} increase was not detected in CAD96CA-M3 and CAD96CA-M4 under JH III-induced (*Figure 5E*), JH III-induced Ca^{2+} mobilization was slightly detected in FGFR1-M3, and JH III-induced Ca^{2+} mobilization was not detected in FGFR1-M4 (*Figure 5F*). These results confirmed that CAD96CA and FGFR1 play roles in transmitting JH III signal.

Discussion

JH regulates insect development through intracellular and membrane signaling; however, the cell membrane receptors and the mechanism are unclear. In this study, CAD96CA and FGFR1 were screened out from the total 20 RTKs in the *H. armiger* genome and identified as JH III cell membrane receptors, which transmit JH signal for gene expression and have a high affinity to JH III.

CAD96CA and FGFR1 transmit JH signal

JH induces a set of gene expression, such as *Kr-h1* (*Truman, 2019*), *Vg (Roy et al., 2018; Song et al., 2014*), *Jhi-1*, and *Jhi-26* (*Dubrovsky et al., 2000*), a rapid calcium increase, phosphorylation of MET and Tai (*Liu et al., 2015*), and prevents pupation. We found several RTKs are involved in JH III-induced gene expression and calcium increase; however, only *Cad96ca*, *Nrk*, *Fgfr1*, and *Wsck* are involved in the JH III-induced pupation delay, in which, only CAD96CA, NRK, and FGFR1 are involved in the JH-induced phosphorylation of MET1 and TAI, and only CAD96CA and FGFR1 can bind JH III. Therefore, CAD96CA and FGFR1 are finally determined as JH III receptors.

CAD96CA (also known as Stitcher, Ret-like receptor tyrosine kinase) activates upon epidermal wounding in *Drosophila* embryos (*Tsarouhas et al., 2014*) and promotes growth and suppresses autophagy in the *Drosophila* epithelial imaginal wing discs (*O'Farrell et al., 2013*). Homozygous *Cad96ca* null *Drosophila* die at late pupal stages (*Wang et al., 2009*). Here, we reported that CAD96CA prevents pupation and transmits JH signal as a JH cell membrane receptor. We also showed that CAD96CA of other insects have universal functions to transmit JH signal to trigger Ca^{2+} mobilization by the study in Sf9 cell lines of *S. frugiperda* and S2 cell lines of *D. melanogaster*.

D. melanogaster FGFRs control cell migration and differentiation in the developing embryo (*Muha and Muller, 2013*). FGF binds FGFR trigger cell proliferation, differentiation, migration, and survival (*Beenken and Mohammadi, 2009; Lemmon and Schlessinger, 2010*). In the mouse, null

mutation of *Fgfr1* or *Fgfr2* is embryonic lethal (*Arman et al., 1998; Deng et al., 1994; Yamaguchi et al., 1994*). In *D. melanogaster* homozygous *Htl* (*Fgfr*) mutant embryos exhibit severe mesoderm spreading defects and die during late embryogenesis (*Beati et al., 2020; Beiman et al., 1996; Gisselbrecht et al., 1996*). In the study, we found that chimeric mutants produced by gene knockout of *Fgfr1* exhibit an early pupation phenotype. The role of FGFR1 in preventing pupation and transmitting JH signal was confirmed in our study. FGFR1 has a similar function to CAD96CA, including transmitting JH signal for *Kr-h1* expression, larval status maintaining, calcium increase, phosphorylation of transcription factors MET1 and TAI, and high affinity to JH III; however, the *Fgfr1* gene is highly expressed in the midgut, possibly it plays a role major in the midgut. In the study, we proved that CAD96CA and FGFR1 transmit JH III signals in three different insect cell lines. In future studies, knockdown of *Cad96ca* and *Fgfr1* in larvae of *S. frugiperda* and *D. melanogaster* will be conducted to detect JH III-induced phosphorylation of MET1 or TAI and its effect on pupation timing.

Other RTKs play roles in JH signaling, and their functions and mechanisms in JH pathway need to be addressed in the future study. This study does not exclude the identification of other RTKs for JH signal transduction by the different screening methods. In addition, GPCRs also play a role in JH signaling. JH triggers GPCR, RTK, PLC, IP3R, and PKC to phosphorylate Na^+/K^+-ATPase-subunit, consequently activating Na^+/K^+-ATPase for the induction of patency in *L. migratoria* vitellogenin follicular epithelium (*Jing et al., 2018*); JH activates a signaling cascade including GPCR, PLC, extracellular Ca^{2+}, and PKC, which induces vitellogenin receptor (VgR) phosphorylation and promotes vitellogenin (Vg) endocytosis in *Locusta migratoria* (*Jing et al., 2021*). JH activates a signaling cascade including GPCR, Cdc42, Par6, and aPKC, leading to an enlarged opening of patency for Vg transport (*Zheng et al., 2022*). In *Tribolium castaneum*, the dopamine D2-like receptor-mediated JH signaling promotes the accumulation of vitellogenin and increases the level of cAMP in oocytes (*Bai and Palli, 2016*). In *H. armigera*, GPCRs are involved in JH III-induced broad isoform 7 (BRZ7) phosphorylation (*Cai et al., 2014*). In summary, these published results indicate that RTKs and GPCRs contribute to JH signaling on the cell membrane, however, the GPCR functions as JH receptor needs to be addressed in the future study. We found that the RNAi of RTKs do not affect JH-induced *Jhi-1* expression, which implies other receptors exist, presenting a target for future study of the new JH III receptor.

The affinity of CAD96CA and FGFR1 to JH III

RTKs are high–affinity cell surface receptors for many cytokines, polypeptide growth factors, and peptide hormones (*Trenker and Jura, 2020*). The ligand of FGFR is FGF of *D. melanogaste*r (*Kadam et al., 2009*); however, the ligand of CAD96CA is currently unknown. The FGFR in the membrane of Sf9 cells can bind to Vip3Aa, confirmed by MST binding affinity assay and co-immunoprecipitation assay (*Jiang et al., 2018*); however, there is no report that RTKs bind lipid hormones. We determined that CAD96CA and FGFR1 have a high affinity to JH III after they are isolated from the cell membrane by MST and ITC methods.

The [^{3}H]JH III detection method is used to determine *Drosophila* MET *in vitro* translation product binding JH III (Kd = 5.3 nM) (*Miura et al., 2005*), and *Tribolium* MET binding JH III (Kd = 2.94 nM) (*Charles et al., 2011*). However, the commercial production of [^{3}H]JH III has ceased, whereas the microscale thermophoresis (MST) method is a widely used method to detect protein binding of small molecules (*Welsch et al., 2017*). Therefore, MST was used in our study as the alternative method to measure the binding strengths of RTKs with JH III. Using the MST method, we determined that the saturable specific binding of *Helicoverpa* MET1 to JH III is Kd of 6.38 nM, which is comparable to that report for *Drosophila* MET and *Tribolium* MET using [^{3}H]JH III, confirming MST method can be used to detect protein binding JH III. The CAD96CA exhibited saturable specific binding to JH III with a Kd of 11.96 nM, and FGFR1 showed a Kd of 23.61 nM, which is higher than that of MET1 for JH III, suggesting lower binding affinity of RTKs than the intracellular receptor MET1 for JH III. A similar phenomenon is reported in another study, the binding affinities of steroid membrane receptors are orders of magnitude lower than those of nuclear receptors (*Falkenstein et al., 2000*). NRK did not bind JH III. One possible explanation is that NRK has a low affinity to JH III and thus transmits JH signal without binding, or alone NRK is

unable to bind JH III and requires the assistance of other proteins. Our study provides new evidence for the binding of lipid hormones by RTK and a new method to study the binding of ligands to receptors.

We also verified the affinity of CAD96CA and FGFR1 with JH III, determining their respective Kd values as 79.6 and 88.5 nanomolar through the ITC method. ITC is a versatile analytical method for the character of molecular interactions (*Johnson, 2021*). ITC is applied in the membrane protein family, containing G protein- coupled receptors, ion channels, and transporters *(Draczkowski et al., 2014*). The ITC method requires relatively high ligand and receptor concentrations for better saturation curves (*Rajarathnam and Rösgen, 2014*). However, when we prepared a protein solution of 1000 nM, protein aggregation occurred, thus we used a protein solution with a concentration of 700 nM. The Kd value detected by ITC is slightly higher than the result of the MST method; the results are sufficient to confirm the high affinity of CAD96CA and FGFR1 binding to JH III.

Although JH I and JH II are natural hormones for lepidopteran larvae (*Furuta et al., 2013; Schooley et al., 1984*), *H. armigera* (*Liu et al., 2013*) and *B. mori (Deng et al., 2011; Kayukawa et al., 2012*) also respond to JH III. In *B. mori* Bm-aff3 cells, the effective concentrations (EC50) of JHs (JH I, JH II, JH III, JHA, or methyl farnesoate) to induce *Kr-h1* transcription are 1.6×10^{-10}, 1.2×10^{-10}, 2.6×10^{-10}, 6.0×10^{-8}, and 1.1×10^{-7} M, respectively (*Kayukawa et al., 2012*). In cultures of wing imaginal discs from *B. mori*, 1–2 μM JH III promotes cuticle protein 4 gene expression (*Deng et al., 2011*). The effective concentration of JH III to induce rapid calcium increase in HaEpi cells is ≥ 1 μM (*Wang et al., 2016*) and 500 ng of 6th instar larva (*Cai et al., 2014*). JH III is a commercial reagent; therefore, we used JH III to carry out the experiments in this study.

Relationship of cell membrane receptor and intracellular receptor

MET is determined as JH intracellular receptor by its characters binding to JH and regulating *Kr-h1* expression (*Charles et al., 2011; Jindra et al., 2021*). In our study, cell membrane receptors CAD96CA and FGFR1 are also able to bind JH III and transmit JH III signal to regulate a set of JH III-induced gene expression including *Kr-h1*. Obviously, both intracellular receptor MET and cell membrane receptor CAD96CA and FGFR1 are involved in JH III signaling as receptors. The study in human cell line HEK293 shows that overexpression of *B. mori* JH intracellular receptor MET2 and its cofactor SRC together in HEK293 cells may activate JH specific kJHRE reporter expression in a JH-dependent way (*Kayukawa et al., 2012*), suggesting JH can diffuse into cells to initiate kJHRE reporter expression by the overexpressed intracellular receptor MET2 and its cofactor SRC in HEK293. Our study also showed that overexpression of CAD96CA or FGFR1 in HEK-293T cells elicits Ca^{2+} elevation, suggesting CAD96CA or FGFR1 transmit JH III signal in HEK-293T cells. The difference is that JH III via MET induces gene expression, whereas, JH III via CAD96CA or FGFR1 induces rapid Ca^{2+} increase. This phenomenon indicates that JH III transmits signal by either cell membrane receptor and intracellular receptor at different stages in the signaling, with cell membrane receptor CAD96CA and FGFR1 inducing rapid Ca^{2+} signaling, which regulates the phosphorylation of MET and TAI to enhance the function of MET for gene transcription *(Liu et al., 2015*), and intracellular receptor MET regulates gene transcription by partial diffusion into cells based its lipid characteristic.

Conclusion

CAD96CA and FGFR1 were involved in JH III signaling, including larval status maintaining, JH III-induced rapid calcium increase, gene expression, and phosphorylation of MET and TAI. CAD96CA and FGFR1 had high affinity to JH III and were possible cell membrane receptors of JH III. CAD96CA and FGFR1 had a general role in transmitting the JH III signal for gene expression in various insect cells. JH III transmits signal by either cell membrane receptor and intracellular receptor at different stages in the signaling, with JH III transmitting the signal by cell membrane receptor CAD96CA and FGFR1 to induce rapid Ca^{2+} signaling, which regulates the phosphorylation of MET and TAI to enhance the function of MET for gene transcription, and intracellular receptor MET regulates gene transcription by partial diffusion into cells based its lipid

392 characteristic (*Figure 6*). This study presents a platform to identify the agonist or inhibitor of JH
393 cell membrane receptors to develop an environmental friend insect growth regulator.

394

Materials and Methods

Experimental insects

Cotton bollworms (*H. armigera*) were raised on an artificial diet comprising wheat germ and soybean powder with various vitamins and inorganic salts. The insects were kept in an insectarium at 26 ± 1 °C with 60 to 70% relative humidity and under a 14 h light:10 h dark cycle.

Cell culture

Our laboratory established the *H. armigera* epidermal cell line (HaEpi) (*Shao et al., 2008*). The cells were cultured as a loosely attached monolayer and maintained at 27 °C in tissue culture flasks. The tissue culture flasks had an area of 25 cm^2 with 4 mL of Grace's medium supplemented with 10% fetal bovine serum (Biological Industries, Cromwell, CT, USA). The Sf9 cell line (Thermo Fisher Scientific, Waltham, Massachusetts, USA) was cultured in ESF921 medium at 27 °C. The S2 cell line was cultured in Schneider's *Drosophila* medium (Gibco, California, USA) with 10% FBS (Sigma, San Francisco, CA, USA) at 27 °C. The cells were subcultured when cells covered 80% of the culture flasks. The HEK-293T cell line was cultured in Dulbecco's Modified Eagle Medium (DMEM, Gibco, California, USA) with 10% FBS (Sigma, St. Louis, Missouri, USA) at 37 °C with 5% carbon dioxide.

Bioinformatic analyses

Identification of RTKs by looking for the name of RTK in the genome of *H. armigera* using bioinformatics. Then, blast analysis was used to search for more RTKs. These RTKs were compared with previously reported RTK species in *B. mori*, *D. melanogaster*, and *H. sapiens* to confirm the amount of RTK in *H. armigera*. The phylogenetic trees were constructed from amino acid sequences using the Neighbor Joining (NJ) method in MEGA 5.0. The structure domains of the proteins were predicted using SMART (http://smart.embl-heidelberg.de/). Although the SMART tool did not predict that the TORSO has a transmembrane structure, the TORSO of *H. armigera* is 79% identity to that of TORSO of RTK members in *B. mori*. We believe that the TORSO of *H. armigera* belongs to the RTK family, but SMART failed to predict its structure successfully. Although the SMART tool did not predict the complete structure of STE20-like, it was clustered with the RTK of CAD96CA in evolutionary tree clustering analysis. In addition, in sequence alignment, the named flocculation protein FLO11-like in *Hyposmocoma kahamanoa* was 85% identity to it, and FLO11-like protein showed transmembrane structure in domain prediction, so the STE20-like of *H. armigera* was classified as a member of the RTK family.

Double-stranded RNA synthesis

RNA interference (RNAi) has been used widely in moths of 10 families (*Xu et al., 2016*). Long double-stranded RNA (dsRNA) can be processed into smaller fragments, with a length of 21–23 nucleotides (*Zamore et al., 2000*), to restrain transcription of the target gene (*Fire et al., 1998*). dsRNA transcription was performed as follows: 2 μg of DNA template, 20 μL of 5 × transcription buffer, 3 μL of T7 RNA polymerase (20 U/μL), 2.4 μL of A/U/C/GTP (10 mM) each, 3 μL of RNase inhibitor (40 U/μL, Thermo Fisher Scientific, Waltham, USA), and RNase-free water were mixed to a volume of 50 μL. After incubation at 37 °C for 4–6 h, 10 μL RNase-free DNase I (1 U/μL, Thermo Fisher Scientific), 10 μL of DNase I Buffer, and 30 μL RNase-free water were added to the solution, which was incubated at 37 °C for 1 h. The solution was extracted with phenol/chloroform and precipitated with ethanol; the precipitate was resuspended with 50 μL RNase-free water. The purity and integrity of the dsRNA was determined using agarose gel electrophoresis. A MicroSpectrophotometer (GeneQuant; Amersham Biosciences, Little Chalfont, UK) was used to quantify the dsRNAs.

RNA interference in HaEpi cells

When the HaEpi cell density reached 70 to 80% in six-well culture plates, the cells were transfected with dsRNA (1 μg/mL) and Quick Shuttle Enhanced transfection reagent (8 μL) (Biodragon Immunotechnologies, Beijing, China) diluted in sterilized saline medium (200 μL), and

incubated with Grace's medium. The cells were cultivated for 48 h at 27 °C. After that, the medium was replaced with a fresh Grace's medium with JH III at a final concentration of 1 μM for 12 h. An equivalent volume of DMSO was a control. The total mRNA was then extracted for qRT-PCR.

RNA interference in larvae

The DNA fragments of *Rtks* were amplified as a template for dsRNA synthesis using the primers RTK-RNAiF and RTK-RNAiR (*Supplementary file 2*). The dsRNAs (*dsRtk*, *dsGFP*) were injected using a micro-syringe into the larval hemocoel of the fifth instar 20 h at 500 ng/larva, using three injections at 36 h intervals. At 12 h after the last injection, 500 ng of JH III (Santa Cruz Biotechnology, Santa Cruz, CA, USA) was injected into each larva. Dimethyl sulfoxide (DMSO) was used as a control. The phenotypes and developmental rates of the larvae were recorded. The mRNA was isolated from the larvae at 12 h after JH III injection.

Protein overexpression

The nucleotide sequence of the genes involved in this study was cloned into the pIEx-4-His, pIEx-4-GFP-His, pIEx-4-CopGFP-His, pcDNA3.1-GFP-His or pcDNA3.1-His vector. The cells were cultured to 80% confluence at 27 °C in the medium. For transfection, approximately 5 μg of plasmids, 200 μL of sterilized saline water medium, and 8 μL of transfection reagent (Biodragon, Beijing, China) were mixed with the cells in the medium for 24–48 h.

Quantitative real–time reverse transcription PCR (qRT–PCR)

Total RNA was extracted from HaEpi cells and larvae using the Trizol reagent (TransGen Biotech, Beijing, China). According to the manufacturer's instructions, first-strand cDNA was synthesized using a 5 × All-In-One RT Master Mix (Abm, Vancouver, Canada). qRT–PCR was then performed using the CFX96 real–time system (Bio-Rad, Hercules, CA, USA). The relative expression levels of the genes were quantified using *Actb* (β-actin) expression as the internal control. The primers are listed in *Supplementary file 2*. The experiments were conducted in triplicate with independent experimental samples. The relative expression data from qRT–PCR were calculated using the formula: $R= 2^{-\Delta\Delta CT}$ ($\Delta\Delta Ct = \Delta Ct_{sample}-\Delta Ct_{control}$, $\Delta Ct = Ct_{gene}-Ct_{\beta\text{-actin}}$) (*Livak and Schmittgen, 2001*).

Detection of the cellular levels of calcium ions

The cells were cultured to a density of 70–80%. The cells were incubated with Dulbecco's phosphate-buffered saline (DPBS) (137 mM NaCl, 2.7 mM KCl, 1.5 mM KH_2PO_4, and 8 mM Na_2HPO_4) including 3 μM acetoxymethyl (AM) ester calcium crimson™ dye (Invitrogen, Carlsbad, CA, USA) for 30 min at 27 °C. The cells were washed with fresh DPBS three times. The cells were then exposed to 1 μM JH III to detect the intracellular calcium concentration. After that, cells in DPBS were treated with Calcium chloride (final concentration 1 mM) and JH III (final concentration 1 μM), and put into a microscope dish. Fluorescence was detected at 555 nm, and the cells were photographed automatically once every 6 s for 420 s using a Carl Zeiss LSM 700 laser scanning confocal microscope (Thornwood, NY, USA). The fluorescence intensity of each image was analyzed using Image Pro-Plus software (Media Cybernetics, Rockville, MD, USA).

Western blotting

Epidermis, midgut, and fat body tissues were homogenized in 500 μL Tris-HCl buffer (40 mM, pH 7.5) on ice with 5 μL phenylmethylsulfonyl fluoride (PMSF, 17.4 mg/mL in isopropyl alcohol), respectively. The homogenate was centrifuged for 15 min at 4 °C at 12,000 × g, then supernatant was collected. The protein concentration in the supernatant was measured using the Bradford protein assay. Proteins (20 μg per sample) sample was subjected to 7.5% or 12.5% SDS-PAGE and transferred onto a nitrocellulose membrane. The membrane was incubated in blocking buffer (Tris-buffered saline, 150 mM NaCl, 10 mM Tris-HCl, pH 7.5, with 3–5% fat-free powdered milk) for 1 h at room temperature. The primary antibody was diluted in blocking buffer, then incubated with the membrane at 4 °C overnight. The membrane was washed three times wash with TBST

(0.02% tween in TBS) for 10 min each. Subsequently, the membrane was incubated with secondary antibodies, 1:10,000 diluted, alkaline phosphatase-conjugated (AP) or horseradish peroxidase-conjugated (HRP) AffiniPure Goat Anti-Rabbit/-Mouse IgG (ZSGB-BIO, Beijing, China). The membrane was washed twice with TBST and once with TBS. The immunoreactive protein bands marked by AP were observed after incubating in 10 mL of TBS solution combined with 45 μL of P-nitro-blue tetrazolium chloride (NBT, 75 μg/μL) and 30 μL of 5-bromo-4-chloro-3 indolyl phosphate (BCIP, 50 μg/μL) in the dark for 10–30 min. The reactions were stopped by washing the membrane with deionized water and images by the scanner. The proteins marked by HRP were detected using a High-Sig ECL Western Blotting Substrate and exposed to a Chemiluminescence imaging system (Tanon, Shanghai, China), according to the manufacturer's instructions. The immunoreactive protein band density was calculated using ImageJ software (National Institutes of Health, Bethesda, MD, USA). The data were analyzed using GraphPad Prism 5 software (GraphPad Software, San Diego, CA, USA).

Lambda protein phosphatase (λPPase) treatment

The protein suspension (40 μL, 0.1 mg/mL) was incubated with λPPase (0.5 μL), buffer (5 μL), and $MnCl_2$ (5 μL) at 30 °C for 30 min, according to the manufacturer's specifications (New England Biolabs, Beijing LTD, Beijing, China). Total proteins were subjected to SDS-PAGE and then electrophoretically transferred onto a nitrocellulose membrane for western blotting.

Phos-tag SDS-PAGE

Phos-tag Acrylamide (20 μM; Fujiflm Wako Pure Chemical Corporation, Osaka, Japan) and $MnCl_2$ (80 μM) were mixed into a normal SDS-PAGE gel. The phosphates of the phosphorylated protein can bind to Mn^{2+}, which reduces the mobility of the phosphorylated protein in the gel. The protein sample was treated with 20% trichloroacetic acid (TCA) to remove the chelating agent. The gel was shaken and incubated three times in 10 mmol/L EDTA transfer buffer solution for Phos-tag SDS-PAGE for 10 min each time. Mn^{2+} was removed, and then the proteins were electrophoretically transferred to a nitrocellulose membrane and analyzed using western blotting.

Immunocytochemistry

The cells were grown on coverslips, treated with hormones, washed three times with DPBS, and fixed using 4% paraformaldehyde in PBS for 10 min in the dark. The fixed cells were incubated with 0.2% Triton-X 100 diluted in PBS for 10 min. The cells were washed with DPBS five times for 3 min each, and the plasma membrane was stained with Alexa Fluor 594-conjugated wheat germ agglutinin (WGA) (1:2,000 in PBS) (Invitrogen, Carlsbad, CA, USA) for 8 min. The cells were washed with DPBS five times for 3 min each, and stained with 4', 6-diamidino-2-phenylindole (DAPI, 1 μg/mL in PBS) (Sigma, San Francisco, CA, USA) in the dark at room temperature for 8 min. The fluorescence signal was detected using an Olympus BX51 fluorescence microscope (Olympus, Tokyo, Japan). Scale bar = 20 μm.

Mutations of CAD96CA and FGFR1

The structures of CAD96CA and FGFR1 were predicted online with SMART. According to the location of the predicted domain, the target fragment was amplified with mutated primers (*Supplementary file 2*) and cloned into the pIEx-4-CopGFP-His vector or pcDNA3.1-GFP-His. The CAD96CA mutants were constructed to CAD96CA-M1-CopGFP-His (AA: 51-615) CAD96CA-M2-CopGFP-His (AA: 101-615) CAD96CA-M1-CopGFP-His (AA: 151-615) and CAD96CA-M1-CopGFP-His (AA: 201-615). FGFR1 mutants were constructed to FGFR1-M1-GFP-His (AA: 101-615), FGFR1-M2-GFP-His (AA: 201-615), and FGFR1-M3-GFP-His (AA: 301-615) and FGFR1-M4-GFP-His (AA: 401-615).

Detection of RTK binding JH III by microscale thermophoresis

RTKs and MET1 were recombined in plasmid pIEx-4-CopGFP-His, which was overexpressed in Sf9 cells. After 48 h, total plasma membrane RTKs were extracted using a cell transmembrane

protein extraction kit (BestBio, Shanghai, China). MET1-CopGFP-His and CopGFP-His were extracted using radioimmunoprecipitation assay (RIPA) lysis buffer (20 mM Tris-HCl, pH 7.5; 150 mM NaCl; and 1% Triton X-100) without ethylenediaminetetraacetic acid (EDTA) (Beyotime, Shanghai, China). A 100 μL of slurry of chelating Sepharose with Ni^{2+} was washed three times with binding buffer (500 mM NaCl; 20 mM Tris-HCl, pH 7.9; and 5 mM imidazole) for 5 min. The overexpressed proteins were bound to the washed Ni^{2+}-chelating Sepharose (GE Healthcare, Pittsburgh, PA, USA). The suspension was mixed on a three-dimensional rotating mixer for 40 min at 4 °C. Then, the resin was washed three times for 5 min each time with wash buffer (0.5 M NaCl; 20 mM Tris-HCl, pH 7.9; and 20 mM imidazole). After centrifugation at 500 × *g* for 3 min at 4 °C, the RTKs were washed three times with wash buffer for 5 min each time. The RTKs were eluted using 100 μL of elution buffer (0.5 M NaCl; 20 mM Tris-HCl, pH 7.9; 100 mM imidazole; and 0.5% Triton X-100) and then diafiltration was carried out three times with PBST (PBS, 0.05% Tween, and 0.5% Triton X-100) buffer using Amicon Ultra 0.5 (Merck Millipore, Temecula, CA, USA) to reduce the concentration of imidazole in preparation for the subsequent experiment. The concentration of the isolated RTK was detected using a BCA protein assay kit (Beyotime, Shanghai, China). JH III bound by 50 nM RTK was detected using the microscale thermophoresis (MST) method (Huang and Zhang, 2021; Welsch et al., 2017). Firstly, the fluorescence intensity and the homogeneity of the protein solution were detected. We confirmed that the fluorescence intensity of the protein samples was within the range of the instrument, and there was no aggregation of the protein samples. Then, we carried out experiments. 16 microtubes were prepared, and the ligand was diluted for use at the initial concentration of 1 μM JH III. Specifically, 5 μL of the ligand buffer was added to prepared microtubes No. 2-16. After, 10 μL of the ligand was added to tube No. 1, 5 μL of the ligand solution in tube No. 1 was pipetted out of tube No. 1, added to tube No. 2, and mixed well. Then 5 μL of solution was pipetted from tube No. 2 and added to tube No. 3. Finally, 5 μL of mixed liquid was removed from tube No. 16 and discarded. (The original concentration of JH III was dissolved in DMSO, and therefore, DMSO needed to be added to the ligand dilution buffer to ensure an equal amount of DMSO in each tube). Then, 5 μL of the fluorescence molecule (target protein) was added to each tube and mixed well. With each tube holding a 10 μL volume in total, the tubes were incubated at 4 °C for 30 to 60 minutes. Finally, samples were removed with a capillary tube and tested with an MST Monolith NT.115 (NanoTempers, Munich, Germany).

Detection of RTK binding JH III by isothermal titration calorimetry

The protein purification method was described in the MST experiment. The isothermal titration calorimetry (ITC) assay was performed using MicroCal PEAQ-ITC (Malvern Panalytical, Malvern, U.K.). JH III was dissolved in ethanol, JH III stock solution to a final concentration of 10 μM with PBST buffer. The protein solution with same concentration ethanol, make sure the buffer identity. According to the manufacturer's instructions, JH III (10 μM) was loaded in a syringe, and the protein solution (700 nM) was injected into the ITC cell. Injection of 3 μl of JH III solution over a period of 150 s at a stirring speed of 750 rpm was performed. For the control test, JH III solution was pumped into syringe, and the buffer was injected into the ITC cell. For the data, the experimental data were subtracted with that from the control test by analysis software.

Methyl farnesoate, farnesol, methoprene binding assays, and competition assays

Methyl farnesoate (Echelon Biosciences, Utah, USA), farnesol (Sigma, San Francisco, CA, USA), and methoprene (Sigma, San Francisco, CA, USA) were dissolved in DMSO, respectively, diluted to the corresponding concentration, and the experimental method as described by the MST method for detection of binding. The competitive binding by MST requires fluorescent labeling of ligands (JH III). Currently, there is no suitable method to label JH III, and we only have fluorescently labeled receptors (target protein). The binding curve of adding both JH III and methoprene, but the maximum concentration of JH used in the experiment was 50 nM, while the concentration of methoprene was increasing. The Kd value is generated automatically by the software of the instrument.

Generation of *Cad96ca* or *Fgfr1* edited *H. armigera* using the CRISPR/Cas9 system

The gRNAs were designed using the CRISPRscan tool (https://www.crisprscan.org/?page=sequence) (*Zhang et al., 2021*) and each consisted of an ~20-nucleotide (nt) region in complementary reverse to one strand of the target DNA (protospacer) with an NGG motif at the 3' end (PAM) of the target site and a GGN at position (5' end) of the T7 promoter. The sgRNA primer and universal primer were used as corresponding templates to obtain amplification products. Product transcription was carried out with a T7 Transcription Kit (Thermo Fisher Scientific, Waltham, USA) following the manufacturer's instructions.

Freshly laid eggs on gauze (within 2 h) were collected from gauze using 0.1% (v/v) 84 solution and rinsed with distilled water. The eggs were affixed onto microscope slides using double-sided adhesive tape (Zuo et al., 2017; Zuo et al., 2018). A mixture of 100 ng/μL Cas9 protein (GenScript, New Jersey, USA) and 300 ng/μL gRNA for the injection into the eggs (per egg 2 nL was injected) within 4 h of oviposition using a Pico-litre Microinjector (Warner Instruments, Holliston, USA) (Hou et al., 2021). The injected eggs were incubated at 26 ± 1 °C with 60 to 70% relative humidity for 3–4 days until they hatched. To detect the mutagenesis of *H. armigera* induced by CRISPR/Cas9, we used PCR to amplify the targeted genomic region obtained from fresh epidermis samples of larvae moulted from G0 individuals and used primers at approximately 50-200 base pairs upstream and downstream from the expected double strand break site by HiFi DNA Polymerase (Transgen, Beijing, China). The corresponding PCR products were sequenced, and the PCR fragments from the mutant animals were ligated into a pMD19-T vector (TaKaRa, Osaka, Japan) in preparation for sequencing. The mutated sites were identified by comparison with the wild-type sequence. To detect off-target activity of the CRISPR/Cas9 system-created *Cad96ca* and *Fgfr1* mutants, we searched the *H. armigera* genome for homologues of the target sequences of *Cad96ca* and *Fgfr1* and found that the genes possibly included similar target sequences. PCR amplification and sequencing were performed with these genes.

Generation of *Cad96ca*- or *Fgfr1*-mutant HaEpi cells using the CRISPR/Cas9 system

The target sites were selected according to the CRISPRscan tool (*Supplementary file 2*). Then, two complementary oligonucleotides were synthesized according to the target sequences, and the annealed fragments were cloned into a pUCm-T-U6-gRNA plasmid after forming double chains. Primers gRNAwf-F and gRNAwf-R were used for PCR amplification with the pUCm-T-U6-gRNA plasmid carrying with target gRNA sequence as a template. The obtained fragment was cloned into a pIEx-Cas9-GFP-P2A-Puro plasmid, and pIEx-4-BmU6-gRNA-Cas9-GFP-P2A-Puro was successfully constructed. The pIEx-4-BmU6-Cad96ca-gRNA-Cas9-GFP-P2A-Puro or pIEx-4-BmU6-*Fgfr1*-gRNA-Cas9-GFP-P2A-Puro recombinant vectors were transfected into HaEpi cells with transfection reagent (Roche, Basel, Switzerland). After 48 h of vector transfection (cells can be observed to express green fluorescent protein), fresh medium containing puromycin (Solarbio, Beijing, China) (15 μg/mL) was added to the cells, the medium containing puromycin was replaced every two days until the green fluorescence was gone (about five days), and the medium was replaced. The puromycin-screened cells were used for subsequent experiments. Messy peak figures reporting the results of DNA sequencing showed mutations induced by CRISPR/Cas9 in the HaEpi cells.

Detection of the cellular levels of calcium ions as indicated by protein calcium-sensing GCaMPs

GCaMPs are the most widely used protein calcium sensors (*Dana et al., 2019*). The CMV promoter of pCMV-GCaMP5G was replaced with an IE promoter and transformed into pIE-GCaMP5G, which can be expressed in HaEpi cells. pIE-GCaMP5G was transfected into normal HaEpi cells, *Cad96ca*- and *Fgfr1*-mutant HaEpi cells for 48 h and incubated with JH III (1 μM) or JH III (1 μM) plus $CaCl_2$ (1 mM) for 60 s. First, the cells were photographed in white light and then imaged with a fluorescence microscope.

Calcium levels were detected by Flow-8 AM fluorescence probe

Intracellular calcium levels in Sf9 cells, S2 cells, and HEK-293T cells were determined using the fluorescent probe Fluo-8 AM (MKBio, Shanghai, China). Cells were seeded overnight at 50,000 cells per 100 μL per well in a 96-well black wall/clear bottomed plate. The Fluo-8 dye was diluted to 2 μM with DPBS, while the 20% PluronicF-127 solution was added for a final concentration of 0.02%. Add 100 μl Fluo-8 dye solution to each well. Then the plate was incubated at room temperature for 30 min. The cells were washed with DPBS three times. After JH III was added to the cells, fluorescence intensities were measured using an ENSPIE plate reader (PE, New York, USA) with a filter set of Ex/Em = 490/514 nm.

Antibodies

The sources of the antibodies: anti-His monoclonal antibody, anti-GFP monoclonal antibody, anti-ACTB polyclonal antibodies (ABclonal, Wuhan, China).

Statistical analysis

All data were from at least three biologically independent experiments. The western blotting results were quantified using ImageJ software (NIH, Bethesda, MA, USA). The fluorescence intensity of each image of calcium detection was analyzed using Image Pro-Plus software (Media Cybernetics, Rockville, MD, USA). GraphPad Prism 7 was used for data analysis and results figures (GraphPad Software Inc., La Jolla, CA, USA). Multiple sets of data were compared by analysis of variance (ANOVA). The different lowercase letters show significant differences. Two group datasets were analyzed using a two-tailed Student's *t* test. Asterisks indicate significant differences between the groups (*$p < 0.05$, **$p < 0.01$). Error bars indicate the standard deviation (SD) of three independent experiments.

Acknowledgments

We thank Jingyao Qu, Zhifeng Li, and Jing Zhu at the State Key Laboratory of Microbial Technology, Shandong University for their help in using MST Monolith NT.115. We thank Xiangmei, Ren at the State Key Laboratory of Microbial Technology, Shandong University for help with using ENSPIE plate reader.

Funding

This study was supported by the National Natural Science Foundation of China (grant nos. 32330011 and 32270507).

Data and materials availability

All data are available in the main text and the supplementary information.

Author Contributions

Yan-Xue Li, Conceptualization, Data curation, Investigation, Visualization, Methodology, Writing - original draft; Xin-Le Kang, Software, Investigation; Yan-Li Li, Software, Methodology; Xiao-Pei Wang, Methodology; Qiao Yan, Investigation; Jin-Xing Wan, Conceptualization, Writing - review and editing; Xiao-Fan Zhao, Conceptualization, Funding acquisition, Writing - original draft, Writing - review and editing

Competing Interest Statement

The following authors have previously disclosed a patent application that is relevant to this manuscript: Xiao-Fan Zhao, Yan-Xue Li, and Jin-Xing Wang. The remaining authors declare no competing interests.

References

Alexandratos A, Moulos P, Nellas I, Mavridis K, Dedos SG. 2016. Reassessing ecdysteroidogenic cells from the cell membrane receptors' perspective. *Sci Rep* **6**:20229. DOI: https://doi.org/10.1038/srep20229, PMID: 26847502

Arman E, Haffner-Krausz R, Chen Y, Heath JK, Lonai P. 1998. Targeted disruption of fibroblast growth factor (FGF) receptor 2 suggests a role for FGF signaling in pregastrulation mammalian development. *Proc Natl Acad Sci U S A* **95**:5082-5087. DOI: https://doi.org/10.1073/pnas.95.9.5082, PMID: 9560232

Bai H, Palli SR. 2016. Identification of G protein-coupled receptors required for vitellogenin uptake into the oocytes of the red flour beetle, *Tribolium castaneum*. *Sci Rep* **6**:1-10. DOI: https://doi.org/10.1038/srep27648, PMID: 27277501

Beati H, Langlands A, Ten Have S, Muller HJ. 2020. SILAC-based quantitative proteomic analysis of *Drosophila* gastrula stage embryos mutant for fibroblast growth factor signalling. *Fly (Austin)* **14**:10-28. DOI: https://doi.org/10.1080/19336934.2019.1705118, PMID: 31873056

Beenken A, Mohammadi M. 2009. The FGF family: biology, pathophysiology and therapy. *Nat Rev Drug Discov* **8**:235-253. DOI: https://doi.org/10.1038/nrd2792, PMID: 19247306

Beiman M, Shilo BZ, Volk T. 1996. Heartless, a *Drosophila* FGF receptor homolog, is essential for cell migration and establishment of several mesodermal lineages. *Genes Dev* **10**:2993-3002. DOI: https://doi.org/10.1101/gad.10.23.2993, PMID: 8957000

Cai MJ, Liu W, Pei XY, Li XR, He HJ, Wang JX, Zhao XF. 2014. Juvenile hormone prevents 20-hydroxyecdysone-induced metamorphosis by regulating the phosphorylation of a newly identified broad protein. *J Biol Chem* **289**:26630-26641. DOI: https://doi.org/10.1074/jbc.M114.581876, PMID: 25096576

Charles JP, Iwema T, Epa VC, Takaki K, Rynes J, Jindra M. 2011. Ligand-binding properties of a juvenile hormone receptor, methoprene-tolerant. *Proc Natl Acad Sci U S A* **108**:21128-21133. DOI: https://doi.org/10.1073/pnas.1116123109, PMID: 22167806

Comas D, Piulachs MD, Bellés X. 1999. Fast induction of vitellogenin gene expression by juvenile hormone III in the cockroach *Blattella germanica* (L.) (Dictyoptera, Blattellidae). *Insect Biochem Mol Biol* **29**:821-827. DOI: https://doi.org/10.1016/s0965-1748(99)00058-2, PMID: 10510500

Dana H, Sun Y, Mohar B, Hulse BK, Kerlin AM, Hasseman JP, Tsegaye G, Tsang A, Wong A, Patel R, Macklin JJ, Chen Y, Konnerth A, Jayaraman V, Looger LL, Schreiter ER, Svoboda K, Kim DS. 2019. High-performance calcium sensors for imaging activity in neuronal populations and microcompartments. *Nat Methods* **16**:649-657. DOI: https://doi.org/10.1038/s41592-019-0435-6, PMID: 31209382

Davey KG. 2000. The modes of action of juvenile hormones: some questions we ought to ask. *Insect Biochem Mol Biol* **30**:663-669. DOI: https://doi.org/10.1016/S0965-1748(00)00037-0, PMID: 10876109

Deng CX, Wynshaw-Boris A, Shen MM, Daugherty C, Ornitz DM, Leder P. 1994. Murine FGFR-1 is required for early postimplantation growth and axial organization. *Genes Dev* **8**:3045-3057. DOI: https://doi.org/10.1101/gad.8.24.3045, PMID: 8001823

Deng H, Zheng S, Yang X, Liu L, Feng Q. 2011. Transcription factors BmPOUM2 and BmbetaFTZ-F1 are involved in regulation of the expression of the wing cuticle protein gene BmWCP4 in the silkworm, *Bombyx mori*. *Insect Mol Biol* **20**:45-60. DOI: https://doi.org/10.1111/j.1365-2583.2010.01041.x, PMID: 20825506

Draczkowski P, Matosiuk D, Jozwiak K. 2014. Isothermal titration calorimetry in membrane protein research. *J Pharm Biomed Anal* **87**:313-325. DOI: https://doi.org/10.1016/j.jpba.2013.09.003, PMID: 24119484

Dubrovsky EB, Dubrovskaya VA, Bilderback AL, Berger EM. 2000. The isolation of two juvenile hormone-inducible genes in *Drosophila melanogaster*. *Dev Biol* **224**:486-495. DOI: https://doi.org/10.1006/dbio.2000.9800, PMID: 10926782

Falkenstein E, Tillmann HC, Christ M, Feuring M, Wehling M. 2000. Multiple actions of steroid hormones--a focus on rapid, nongenomic effects. *Pharmacol Rev* **52**:513-556. PMID: 11121509

Feng Q-L, Ladd TR, Tomkins BL, Sundaram M, Sohi SS, Retnakaran A, Davey KG, Palli SR.

1999. Spruce budworm (Choristoneura fumiferana) juvenile hormone esterase: hormonal regulation, developmental expression and cDNA cloning. *Mol Cell Endocrinol* **148**:95-108. DOI: https://doi.org/10.1016/s0303-7207(98)00228-7, PMID: 10221775

Fire A, Xu S, Montgomery MK, Kostas SA, Driver SE, Mello CC. 1998. Potent and specific genetic interference by double-stranded RNA in *Caenorhabditis elegans*. *Nature* **391**:806-811. DOI: https://doi.org/10.1038/35888, PMID: 9486653

Furuta K, Ichikawa A, Murata M, Kuwano E, Shinoda T, Shiotsuki T. 2013. Determination by LC-MS of juvenile hormone titers in hemolymph of the silkworm, *Bombyx mori*. *Biosci Biotechnol Biochem* **77**:988-991. DOI: https://doi.org/10.1271/bbb.120883, PMID: 23649254

Gao Y, Liu S, Jia Q, Wu L, Yuan D, Li EY, Feng Q, Wang G, Palli SR, Wang J, Li S. 2022. Juvenile hormone membrane signaling phosphorylates USP and thus potentiates 20-hydroxyecdysone action in Drosophila. *Sci Bull (Beijing)* **67**:186-197. DOI: https://doi.org/10.1016/j.scib.2021.06.019, PMID: 36546012

Gisselbrecht S, Skeath JB, Doe CQ, Michelson AM. 1996. Heartless encodes a fibroblast growth factor receptor (DFR1/DFGF-R2) involved in the directional migration of early mesodermal cells in the *Drosophila* embryo. *Genes Dev* **10**:3003-3017. DOI: https://doi.org/10.1101/gad.10.23.3003, PMID: 8957001

Honegger AM, Kris RM, Ullrich A, Schlessinger J. 1989. Evidence that autophosphorylation of solubilized receptors for epidermal growth factor is mediated by intermolecular cross-phosphorylation. *Proc Natl Acad Sci U S A* **86**:925-929. DOI: https://doi.org/10.1073/pnas.86.3.925, PMID: 2915986

Hou L, Guo S, Wang Y, Nie X, Yang P, Ding D, Li B, Kang L, Wang X. 2021. Neuropeptide ACP facilitates lipid oxidation and utilization during long-term flight in locusts. *Elife* **10:** e65279. DOI: https://doi.org/10.7554/eLife.65279, PMID: 34151772

Huang L, Zhang C, 2021. Microscale thermophoresis (MST) to detect the interaction between purified protein and small molecule. *Methods Mol Biol* **2213**:187-193. DOI: https://doi.org/10.1007/978-1-0716-0954-5_17, PMID: 33270204

Jiang K, Hou X, Han L, Tan T, Cao Z, Cai J. 2018. Fibroblast growth factor receptor, a novel receptor for vegetative insecticidal protein Vip3Aa. *Toxins (Basel)* **10:**546. DOI: https://doi.org/10.3390/toxins10120546, PMID: 30567360

Jindra M, Tumova S, Milacek M, Bittova L, 2021. A decade with the juvenile hormone receptor. *Adv. Insect. Physiol.* **60**:37-85. https://doi.org/10.1016/bs.aiip.2021.03.001

Jing YP, An H, Zhang S, Wang N, Zhou S. 2018. Protein kinase C mediates juvenile hormone–dependent phosphorylation of Na^+/K^+-ATPase to induce ovarian follicular patency for yolk protein uptake. *J Biol Chem* **293**:20112-20122. DOI: https://doi.org/10.1074/jbc.RA118.005692, PMID: 30385509

Jing YP, Wen X, Li L, Zhang S, Zhang C, Zhou S. 2021. The vitellogenin receptor functionality of the migratory locust depends on its phosphorylation by juvenile hormone. *Proc Natl Acad Sci U S A* **118**. DOI: https://doi.org/10.1073/pnas.2106908118, PMID: 34493670

Johnson CM. 2021. Isothermal titration calorimetry. *Methods Mol Biol* **2263**:135-159. DOI: https://doi.org/10.1007/978-1-0716-1197-5_5, PMID: 33877596

Kadam S, McMahon A, Tzou P, Stathopoulos A. 2009. FGF ligands in *Drosophila* have distinct activities required to support cell migration and differentiation. *Development* **136**:739-747. DOI: https://doi.org/10.1242/dev.027904, PMID: 19158183

Kayukawa T, Minakuchi C, Namiki T, Togawa T, Yoshiyama M, Kamimura M, Mita K, Imanishi S, Kiuchi M, Ishikawa Y, Shinoda T. 2012. Transcriptional regulation of juvenile hormone-mediated induction of Krüppel homolog 1, a repressor of insect metamorphosis. *Proc Natl Acad Sci U S A* **109**:11729-11734. DOI: https://doi.org/10.1073/pnas.1204951109, PMID: 22753472

Konopova B, Jindra M. 2007. Juvenile hormone resistance gene methoprene-tolerant controls entry into metamorphosis in the beetle *Tribolium castaneum*. *Proc Natl Acad Sci U S A* **104**:10488-10493. DOI: https://doi.org/10.1073/pnas.0703719104, PMCID: PMC1965540

Lemmon MA, Schlessinger J. 2010. Cell signaling by receptor tyrosine kinases. *Cell* **141**:1117-1134. DOI: https://doi.org/10.1016/j.cell.2010.06.011, PMID: 20602996

Li M, Mead EA, Zhu J. 2011. Heterodimer of two bHLH-PAS proteins mediates juvenile hormone-

induced gene expression. *Proc Natl Acad Sci U S A* **108**:638-643. DOI: https://doi.org/10.1073/pnas.1013914108, PMID: 21187375

Li YX, Wang D, Zhao WL, Zhang JY, Kang XL, Li YL, Zhao XF. 2021. Juvenile hormone induces methoprene-tolerant 1 phosphorylation to increase interaction with Taiman in *Helicoverpa armigera*. *Insect Biochem Mol Biol* **130**:103519. DOI: https://doi.org/10.1016/j.ibmb.2021.103519, PMID: 33450383

Li Z, Zhou C, Chen Y, Ma W, Cheng Y, Chen J, Bai Y, Luo W, Li N, Du E, Li S. 2022. Egfr signaling promotes juvenile hormone biosynthesis in the *German cockroach*. *BMC Biol* **20**:278. DOI: https://doi.org/10.1186/s12915-022-01484-z, PMID: 36514097

Liu P, Peng HJ, Zhu J. 2015. Juvenile hormone-activated phospholipase C pathway enhances transcriptional activation by the methoprene-tolerant protein. *Proc Natl Acad Sci U S A* **112**:E1871-1879. DOI: https://doi.org/10.1073/pnas.1423204112, PMID: 25825754

Liu W, Zhang FX, Cai MJ, Zhao WL, Li XR, Wang JX, Zhao XF. 2013. The hormone-dependent function of Hsp90 in the crosstalk between 20-hydroxyecdysone and juvenile hormone signaling pathways in insects is determined by differential phosphorylation and protein interactions. *Biochim Biophys Acta* **1830**:5184-5192. DOI: https://doi.org/10.1016/j.bbagen.2013.06.037, PMID: 23850472

Livak KJ, Schmittgen TD. 2001. Analysis of relative gene expression data using real-time quantitative PCR and the 2(-Delta Delta C(T)) method. *Methods* **25**:402-408. DOI: https://doi.org/10.1006/meth.2001.1262, PMID: 11846609

Manning G, Whyte DB, Martinez R, Hunter T, Sudarsanam S. 2002. The protein kinase complement of the human genome. *Science* **298**:1912-1934. DOI: https://doi.org/10.1126/science.1075762, PMID: 12471243

Minakuchi C, Namiki T, Shinoda T. 2009. Krüppel homolog 1, an early juvenile hormone-response gene downstream of methoprene-tolerant, mediates its anti-metamorphic action in the red flour beetle *Tribolium castaneum*. *Dev Biol* **325**:341-350. DOI: https://doi.org/10.1016/j.ydbio.2008.10.016, PMID: 19013451

Minakuchi C, Zhou X, Riddiford LM. 2008. Krüppel homolog 1 (Kr-h1) mediates juvenile hormone action during metamorphosis of *Drosophila melanogaster*. *Mech Dev* **125**:91-105. DOI: https://doi.org/10.1016/j.mod.2007.10.002, PMID: 18036785

Miura K, Oda M, Makita S, Chinzei Y. 2005. Characterization of the *Drosophila* methoprene - tolerant gene product. Juvenile hormone binding and ligand-dependent gene regulation. *FEBS J* **272**:1169-1178. DOI: https://doi.org/10.1111/j.1742-4658.2005.04552.x, PMID: 15720391

Muha V, Muller HA. 2013. Functions and mechanisms of fibroblast growth factor (FGF) signalling in *Drosophila melanogaster*. *Int J Mol Sci* **14**:5920-5937. DOI: https://doi.org/10.3390/ijms14035920, PMID: 23493057

Noriega FG, Shah DK, Wells MA. 2003. Juvenile hormone controls early trypsin gene transcription in the midgut of *Aedes aegypti*. *Insect Mol Biol* **6**:63-66. DOI: https://doi.org/10.1046/j.1365-2583.1997.00154.x, MID: 9013256

O'Farrell F, Wang S, Katheder N, Rusten TE, Samakovlis C. 2013. Two-tiered control of epithelial growth and autophagy by the insulin receptor and the ret-like receptor, stitcher. *PLoS Biol* **11**:e1001612. DOI: https://doi.org/10.1371/journal.pbio.1001612, PMID: 23935447

Ojani R, Liu P, Fu X, Zhu J. 2016. Protein kinase C modulates transcriptional activation by the juvenile hormone receptor methoprene-tolerant. *Insect Biochem Mol Biol* **70**:44-52. DOI: https://doi.org/10.1016/j.ibmb.2015.12.001, PMID: 26689644

Pecasse F, Beck Y, Ruiz C, Richards G. 2000. Krüppel-homolog, a stage-specific modulator of the prepupal ecdysone response, is essential for *drosophila* metamorphosis. *Dev Biol* **221**:53-67. DOI: https://doi.org/10.1006/dbio.2000.9687, PMID: 10772791

Rajarathnam K, Rösgen J. 2014. Isothermal titration calorimetry of membrane proteins — progress and challenges. *Biochim Biophys Acta* **1838**:69-77. DOI: https://doi.org/10.1016/j.bbamem.2013.05.023, PMID: 23747362

Riddiford LM. 2020. Rhodnius, Golden oil, and Met: a history of juvenile hormone research. *Front Cell Dev Biol* **8**:679. DOI: https://doi.org/10.3389/fcell.2020.00679, PMID: 32850806

Roy S, Saha TT, Zou Z, Raikhel AS. 2018. Regulatory pathways controlling female insect

847 reproduction. *Annu Rev Entomol* **63**:489-511. DOI: https://doi.org/10.1146/annurev-ento-020117-
848 043258, PMID: 29058980
849 Schooley DA, Baker FC, Tsai LW, Miller CA, Jamieson GC, 1984. Juvenile Hormones O, I, and II
850 exist only in lepidoptera. In: Hoffmann J., Porchet M. (eds) Biosynthesis, Metabolism and Mode of
851 Action of Invertebrate Hormones. Proceedings in Life Sciences. Springer Berlin Heidelberg,
852 Berlin, Heidelberg. pp 373-383.
853 Shao HL, Zheng WW, Liu PC, Wang Q, Wang JX, Zhao XF. 2008. Establishment of a new cell
854 line from lepidopteran epidermis and hormonal regulation on the genes. *PLoS One* **3**:e3127. DOI:
855 https://doi.org/10.1371/journal.pone.0003127, PMID: 18769621
856 Song J, Wu Z, Wang Z, Deng S, Zhou S. 2014. Krüppel-homolog 1 mediates juvenile hormone
857 action to promote vitellogenesis and oocyte maturation in the migratory locust. *Insect Biochem*
858 *Mol Biol* **52**:94-101. DOI: https://doi.org/10.1016/j.ibmb.2014.07.001, PMID: 25017142
859 Sopko R, Perrimon N. 2013. Receptor tyrosine kinases in *Drosophila* development. *Cold Spring*
860 *Harb Perspect Biol* **5**:a009050. DOI: https://doi.org/10.1101/cshperspect.a009050, PMID:
861 23732470
862 Sparrow LG, McKern NM, Gorman JJ, Strike PM, Robinson CP, Bentley JD, Ward CW. 1997. The
863 disulfide bonds in the C-terminal domains of the human insulin receptor ectodomain. *J Biol Chem*
864 **272**:29460-29467. DOI: https://doi.org/10.1074/jbc.272.47.29460, PMID: 9368005
865 Trenker R, Jura N. 2020. Receptor tyrosine kinase activation: from the ligand perspective. *Curr*
866 *Opin Cell Biol* **63**:174-185. DOI: https://doi.org/10.1016/j.ceb.2020.01.016, PMID: 32114309
867 Truman JW. 2019. The evolution of insect metamorphosis. *Curr Biol* **29**:R1252-R1268. DOI:
868 https://doi.org/10.1016/j.cub.2019.10.009, PMID: 31794762
869 Tsarouhas V, Yao L, Samakovlis C. 2014. Src kinases and ERK activate distinct responses to
870 Stitcher receptor tyrosine kinase signaling during wound healing in *Drosophila*. *J Cell Sci*
871 **127**:1829-1839. DOI: https://doi.org/10.1242/jcs.143016, PMID: 24522188
872 Wang D, Pei XY, Zhao WL, Zhao XF. 2016. Steroid hormone 20-hydroxyecdysone promotes
873 higher calcium mobilization to induce apoptosis. *Cell Calcium* **60**:1-12. DOI:
874 https://doi.org/10.1016/j.ceca.2016.05.003, PMID: 27209368
875 Wang S, Tsarouhas V, Xylourgidis N, Sabri N, Tiklová K, Nautiyal N, Gallio M, Samakovlis C.
876 2009. The tyrosine kinase Stitcher activates Grainy head and epidermal wound healing in
877 *Drosophila*. *Nat Cell Biol* **11**:890-895. DOI: https://doi.org/10.1038/ncb1898, PMID: 19525935
878 Welsch ME, Kaplan A, Chambers JM, Stokes ME, Bos PH, Zask A, Zhang Y, Sanchez-Martin M,
879 Badgley MA, Huang CS, Tran TH, Akkiraju H, Brown LM, Nandakumar R, Cremers S, Yang WS,
880 Tong L, Olive KP, Ferrando A, Stockwell BR. 2017. Multivalent small-molecule Pan-RAS
881 Inhibitors. *Cell* **168**:878-889 e829. DOI: https://doi.org/10.1016/j.cell.2017.02.006, PMID:
882 28235199
883 Wroblewski VJ, Harshman LG, Hanzlik TN, Hammock BD. 1990. Regulation of juvenile hormone
884 esterase gene expression in the tobacco budworm (*Heliothis virescens*). *Arch Biochem Biophys*
885 **278**:461-466. DOI: https://doi.org/https://doi.org/10.1016/0003-9861(90)90285-7, PMID: 2327798
886 Wu Z, Yang L, Li H, Zhou S. 2021. Krüppel-homolog 1 exerts anti-metamorphic and vitellogenic
887 functions in insects via phosphorylation-mediated recruitment of specific cofactors. *BMC Biol*
888 **19**:222. DOI: https://doi.org/10.1186/s12915-021-01157-3, PMID: 34625063
889 Xu J, Wang XF, Chen P, Liu FT, Zheng SC, Ye H, Mo MH. 2016. RNA interference in moths:
890 mechanisms, applications, and progress. *Genes (Basel)* **7**:88. DOI:
891 https://doi.org/10.3390/genes7100088, PMID: 27775569
892 Xu J, Wang YQ, Li ZQ, Ling L, Zeng BS, You L, Chen YZ, Aslam AFM, Huang YP, Tan AJ. 2014.
893 Functional characterization of the vitellogenin promoter in the silkworm, *Bombyx mori*. *Insect.*
894 *Mol. Biol* **23**:550-557. DOI: https://doi.org/10.1111/imb.12102,
895 Yamaguchi TP, Harpal K, Henkemeyer M, Rossant J. 1994. Fgfr-1 is required for embryonic
896 growth and mesodermal patterning during mouse gastrulation. *Genes Dev* **8**:3032-3044. DOI:
897 https://doi.org/10.1101/gad.8.24.3032, PMID: 8001822
898 Yarden Y, Ullrich A. 1988. Molecular analysis of signal transduction by growth factors.
899 *Biochemistry* **27**:3113-3119. DOI: https://doi.org/10.1021/bi00409a001, PMID: 3291942
900 Zamore PD, Tuschl T, Sharp PA, Bartel DP. 2000. RNAi: double-stranded RNA directs the ATP-

dependent cleavage of mRNA at 21 to 23 nucleotide intervals. *Cell* **101**:25-33. DOI: https://doi.org/10.1016/S0092-8674(00)80620-0, PMID: 10778853

Zhang C, Lu T, Zhang Y, Li J, Tarique I, Wen F, Chen A, Wang J, Zhang Z, Zhang Y, Shi DL, Shao M. 2021. Rapid generation of maternal mutants via oocyte transgenic expression of CRISPR-Cas9 and sgRNAs in zebrafish. *Sci Adv* **7**:eabg4243. DOI: https://doi.org/10.1126/sciadv.abg4243, PMID: 34362733

Zhang J, Saleh DS, Wyatt GR. 1996. Juvenile hormone regulation of an insect gene: a specific transcription factor and a DNA response element. *Mol Cell Endocrinol* **122**:15-20. DOI: https://doi.org/10.1016/0303-7207(96)03884-1, PMID: 8898344

Zheng H, Wang N, Yun J, Xu H, Yang J, Zhou S. 2022. Juvenile hormone promotes paracellular transport of yolk proteins via remodeling zonula adherens at tricellular junctions in the follicular epithelium. *PLoS Genet* **18**:e1010292. DOI: https://doi.org/10.1371/journal.pgen.1010292, PMID: 35759519

Zhu J, Chen L, Raikhel AS. 2003. Posttranscriptional control of the competence factor βFTZ-F1 by juvenile hormone in the mosquito *Aedes aegypti*. *Proc Natl Acad Sci U S A* **100**:13338-13343. DOI: https://doi.org/10.1073/pnas.2234416100, PMID: 14593204

Zuo Y, Wang H, Xu Y, Huang J, Wu S, Wu Y, Yang Y. 2017. CRISPR/Cas9 mediated G4946E substitution in the ryanodine receptor of *Spodoptera exigua* confers high levels of resistance to diamide insecticides. *Insect Biochem Mol Biol* **89**:79-85. DOI: https://doi.org/10.1016/j.ibmb.2017.09.005, PMID: 28912111

Zuo YY, Huang JL, Wang J, Feng Y, Han TT, Wu YD, Yang YH. 2018. Knockout of a P-glycoprotein gene increases susceptibility to abamectin and emamectin benzoate in *Spodoptera exigua*. *Insect Mol Biol* **27**:36-45. DOI: https://doi.org/10.1111/imb.12338, PMID: 28753233

Figures

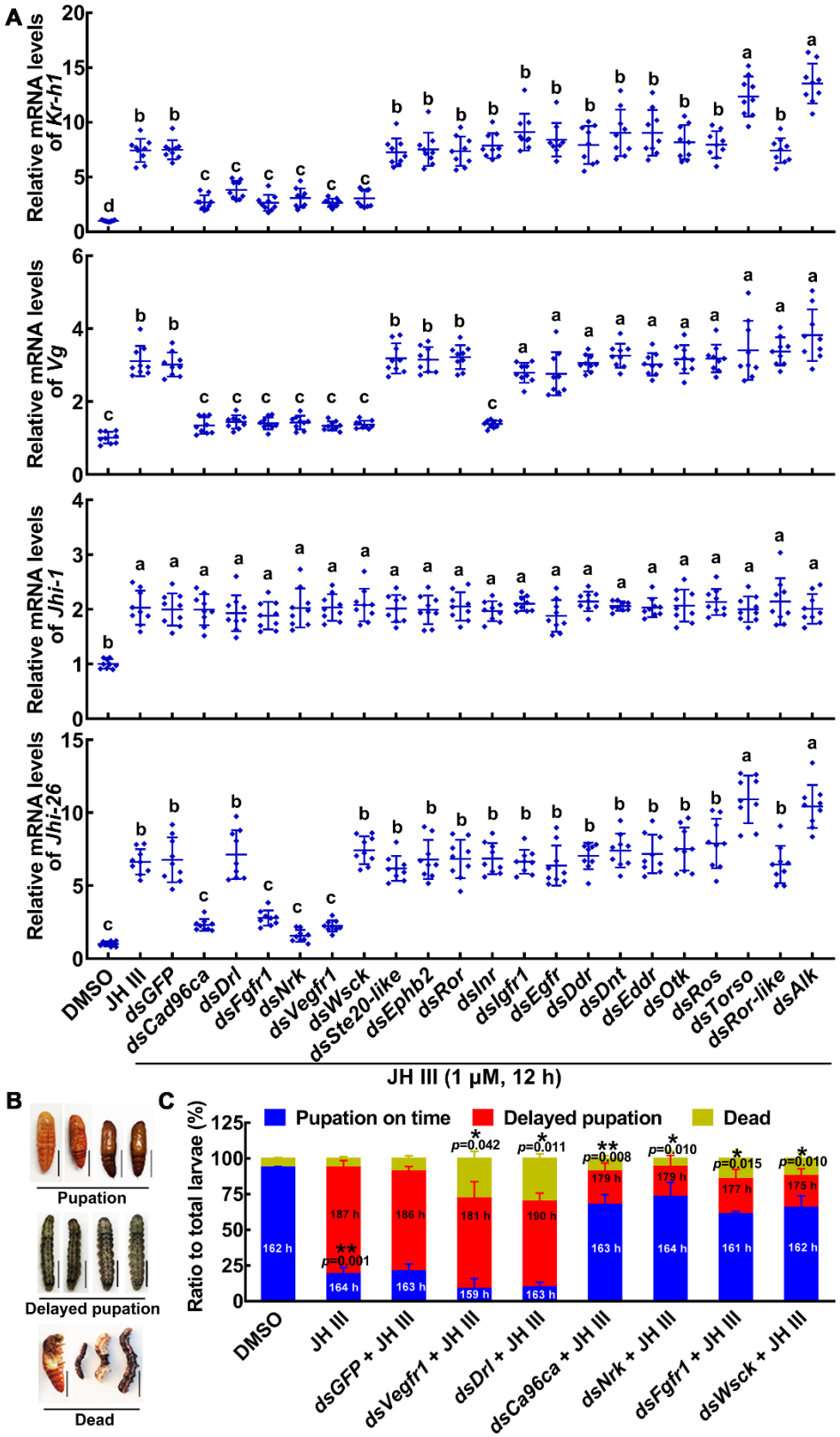

Figure 1. RTKs were screened to determine their involvement in the JH signaling pathway in HaEpi cells and larvae. (**A**) The roles of RTKs in JH III-induced *Kr-h1*, *Vg*, *Jhi-1*, and *Jhi-26* expression were determined by RNAi of *Rtk* genes (1 μg/mL dsRNA, 48 h, 1 μM JH III for 12 h). DMSO as solvent control. The relative mRNA levels were calculated via the $2^{-\Delta\Delta CT}$ method and the bars indicate the mean ± SD. n = 3. Multiple sets of data were compared by analysis of variance (ANOVA). The different lowercase letters show significant differences. (**B**) The examples of phenotype after *Vegfr1*, *Drl*, *Cad96ca*, *Nrk*, *Fgfr1*, and *Wsck* knockdown in larvae. Scale = 1 cm. (**C**) Phenotype percentage and pupation time after *Vegfr1*, *Drl*, *Cad96ca*, *Nrk*, *Fgfr1*, and *Wsck* knockdown in larvae. The time was recorded from the bursting of the head shell of the 5th instar to pupal development. Images were collected after more than 80% of the larvae had pupated in the DMSO control group. Two-group significant differences were calculated using Student's *t* test (**p*<0.05, ***p*<0.01) based on three replicates, n = 30 × 3 larvae.

Figure supplement 1. Phylogenetic tree analysis to identify RTKs of *H. armigera*.

Figure supplement 2. Structural characteristics of the RTK domains.

Figure supplement 3. The interference efficiency of dsRNA and off–target detection.

Figure supplement 4. Expression profiles, interference efficiency and phenotype of 6 *Rtks* in larvae.

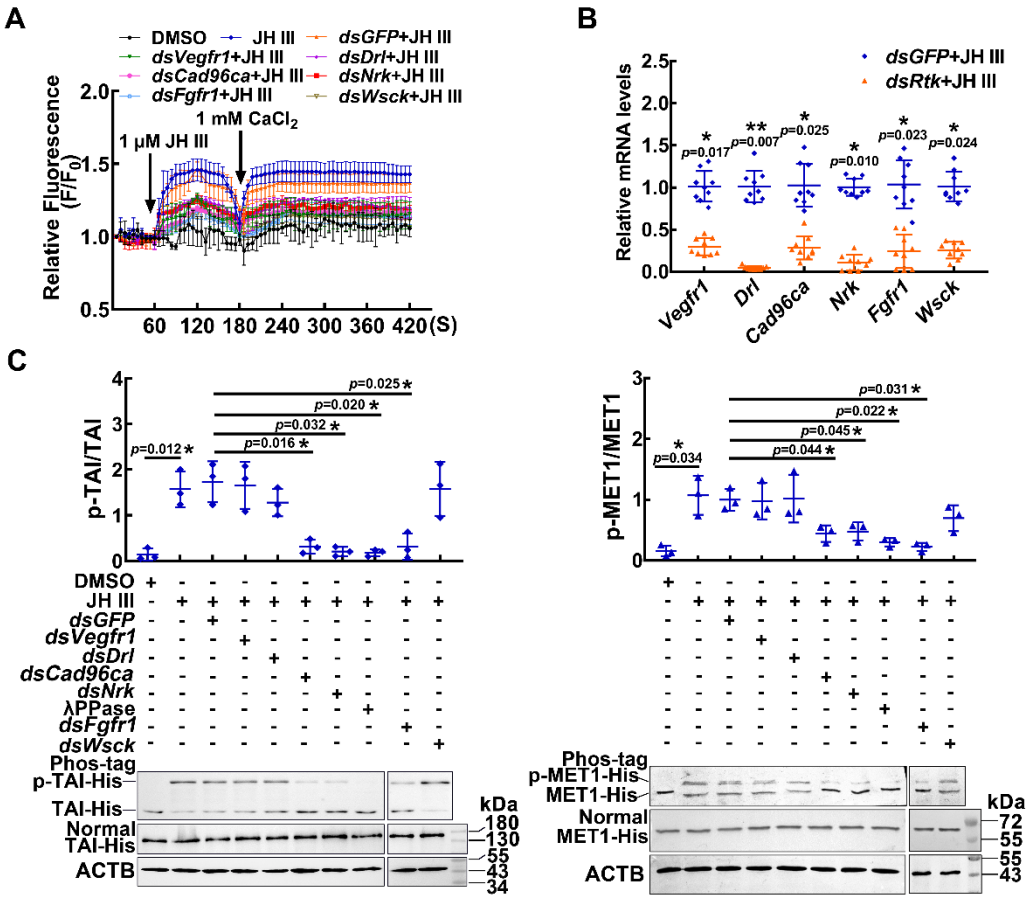

Figure 2. RTKs involved in JH III-regulated Ca^{2+} increase and protein phosphorylation. (**A**) The level of Ca^{2+} after *Vegfr1*, *Drl*, *Cad96ca*, *Nrk*, *Fgfr1*, and *Wsck* knockdown in HaEpi cells. The cells were incubated with dsRNA (the final concentration was 1 μg/mL for 48 h) and AM ester calcium crimson dye (3 μM, 30 min). F_0: the fluorescence intensity of HaEpi cells without treatment. F: the fluorescence intensity of HaEpi cells after different treatments. DMSO as solvent control. (**B**) The interference efficiency of dsRNA in HaEpi cells. (**C**) Western blotting was performed to analyze TAI-His and MET1-His phosphorylation after treatment with dsRNA and JH III (1 μM, 3 h). Phos-tag: phosphate affinity SDS–PAGE gel, Normal: normal SDS–PAGE gel, which was a 7.5 or 10% SDS–PAGE gel. The results of three independent repeated western blots were statistically analyzed by ImageJ software. The *p* value was calculated by Student's *t* test based on three independent replicate experiments.

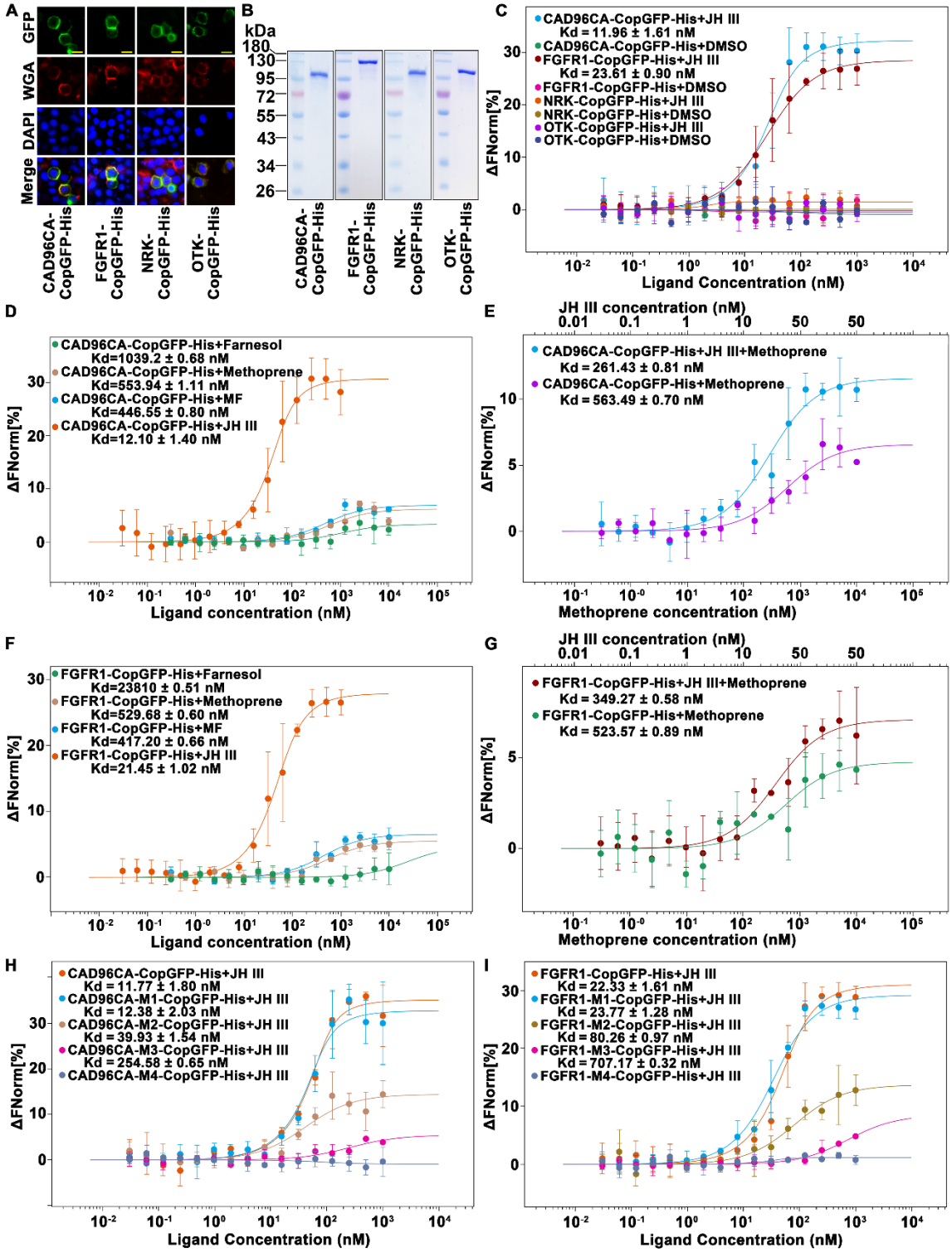

Figure 3. CAD96CA and FGFR1 could bind JH III. (**A**) Cell membrane localization of the overexpressed CAD96CA-CopGFP-His, FGFR1-CopGFP-His, NRK-CopGFP-His and OTK-CopGFP-His. GFP: green fluorescence of RTKs fused with a green fluorescent protein. WGA: red fluorescence, the cell membrane was labeled with wheat germ agglutinin. DAPI: nuclear staining.

Merge: the pictures of different fluorescent-labeled cells were combined. The cells were observed with a fluorescence microscope. Scale bar = 20 μm. (**B**) Coomassie brilliant blue staining of the SDS–PAGE gel showed the purity of the separated CAD96CA-CopGFP-His, FGFR1-CopGFP-His, NRK-CopGFP-His, and OTK-CopGFP-His proteins. (**C**) Saturation binding curves of CAD96CA-CopGFP-His, FGFR1-CopGFP-His, NRK-CopGFP-His and OTK-CopGFP-His. (**D**) Saturation binding curves of CAD96CA-CopGFP-His were incubated with the indicated compounds. (**E**) The binding and competition curves of CAD96CA and methoprene. (**F**) Saturation binding curves of FGFR1-CopGFP-His were incubated with the indicated compounds. (**G**) The binding and competition curves of FGFR1 and methoprene. (**H**) The binding curves of CAD96CA mutants and JH III. (**I**) The binding curves of FGFR1 mutants with JH III. The error line represents three duplicate SD.

Figure supplement 1. MET1 bound JH III, and CAD96CA and FGFR1 mutants.

Figure supplement 2. CAD96CA and FGFR1 bound JH III were analyzed using ITC.

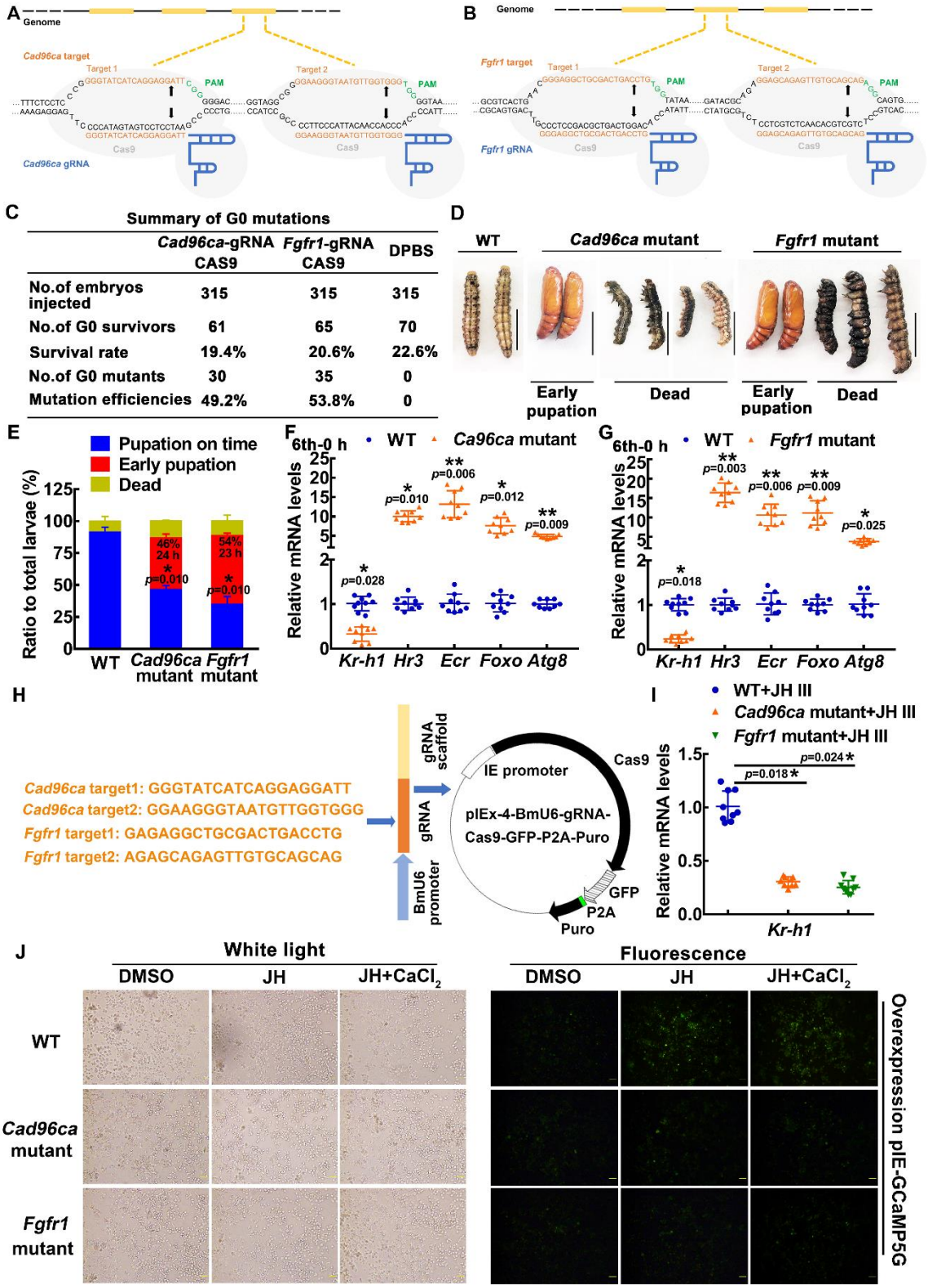

Figure 4. The roles of CAD96CA and FGFR1 in larval development were determined by CRISPR/Cas9 system-mediated mutants. (**A** and **B**) Schematic showing the injection mixture of

the CRISPR/Cas9 system. The black line refers to the genome of *H. armigera*; the yellow blocks correspond to exons. The Cas9 nuclease (in grey) was targeted to genomic DNA by *Cad96ca*-gRNA or *Fgfr1*-gRNA with an ~20-nt guide sequence (orange) and a scaffold (blue). The guide sequence pairs with the DNA target (orange sequence on the top strand), which requires the upstream sequence of the 5'-CGG-3' adjacent motif (PAM; green). Cas9 induces a double-strand break (DSB) ~3 bp upstream of the PAM (black triangle). (**C**) Summary of G0 mutations. (**D**) Images showing WT and mutant *H. armigera* phenotypes. (**E**) Morphology and statistical analysis of WT and mutant *H. armigera*. Both *Cad96ca* and *Fgfr1* mutant larvae showed earlier pupation than WT controls. The scale represents 1 cm. (**F** and **G**) qRT–PCR showing the mRNA levels of the JH/20E response genes in WT and mutant *H. armigera*. (**H**) Schematic showing the CRISPR/Cas9 editing in HaEpi cells by pIEx-4-BmU6-*Cad96ca*-gRNA-Cas9-GFP-P2A-Puro and pIEx-4-BmU6-*Fgfr1*-gRNA-Cas9-GFP-P2A-Puro recombination vectors. (**I**) qRT–PCR showing the mRNA levels of *Kr-h1* in WT and mutant HaEpi cells. (**J**) pIEx-GCaMP5G was overexpressed in WT and mutant HaEpi cells, and calcium mobilization was detected. Green fluorescence shows the calcium signal. The concentration of JH III was 1 μM, and that of $CaCl_2$ was 1 mM. The scale bar represents 100 μm.

Figure supplement 1. Targeted mutagenesis of *Cad96ca* and *Fgfr1* in *H. armigera*.

Figure supplement 2. Targeted mutagenesis of *Cad96ca* and *Fgfr1* in HaEpi cells.

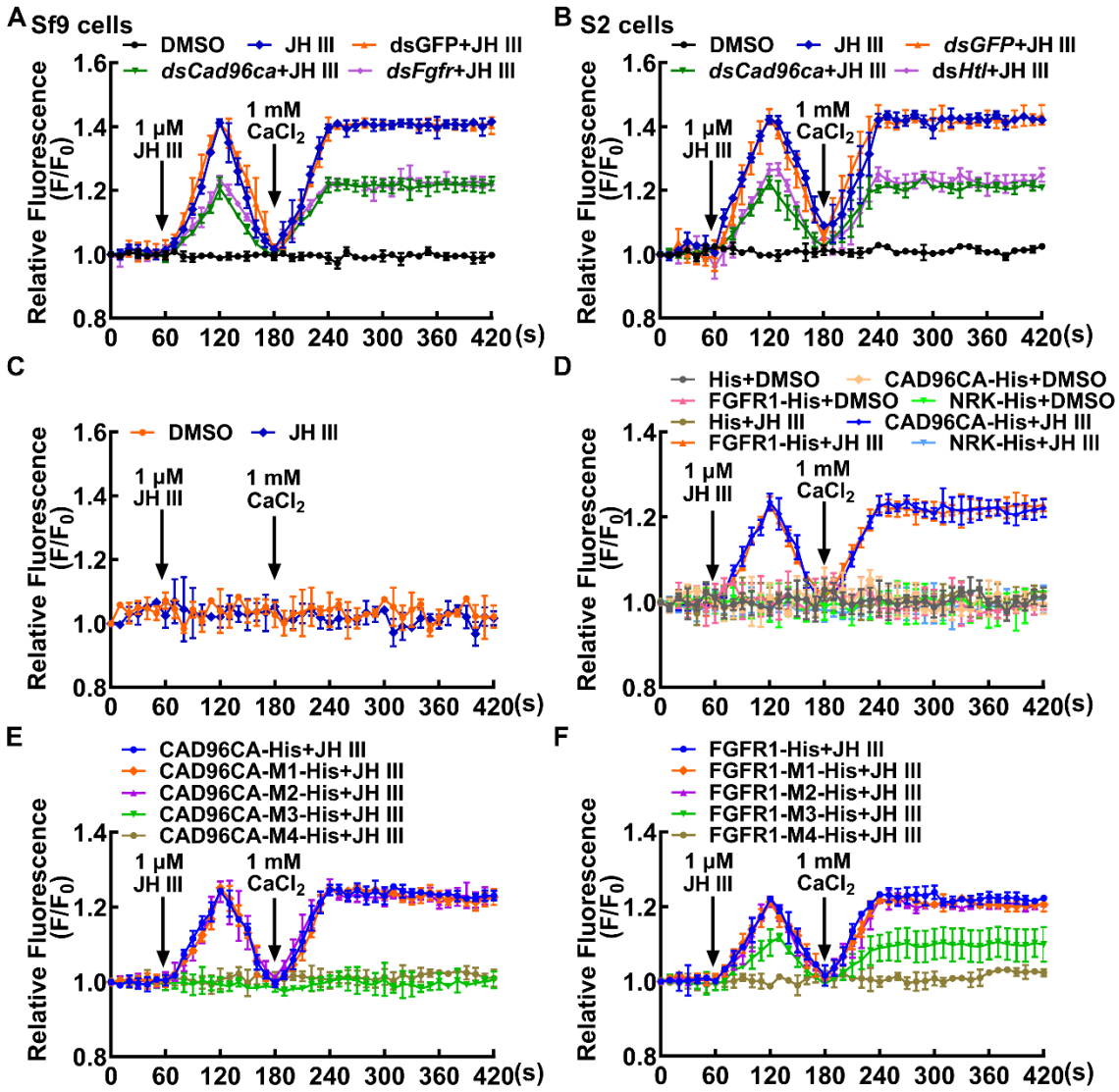

Figure 5. CAD96CA and FGFR1 participated in JH-induced calcium ion mobilization. (**A**) The level of Ca^{2+} after *Cad96ca* and *Fgfr* knockdown in Sf9 cells. The cells were incubated with dsRNA (the final concentration was 1 μg/mL for 48 h). F_0: the fluorescence intensity of Sf9 cells without treatment. F: the fluorescence intensity of Sf9 cells after different treatments. DMSO as solvent control. (**B**) Effect of JH III on calcium ion levels in S2 cells after *Cad96ca* and *Htl* knockdown. (**C**) The response of calcium ion levels to JH III in HEK-293T cells. (**D**) The analysis of calcium ion flow after HEK-293T cells overexpressed RTK. DMSO as solvent control. His as tag control. (**E** and **F**) The calcium was quantitated after HEK-293T cells overexpressed CAD96CA-His, FGFR1-His, and mutants.

Figure supplement 1. The efficiency of the interference experiment was analyzed by qPCR.

Figure supplement 2. CAD96CA, FGFR1 and mutants overexpressed in HEK-293T cells.

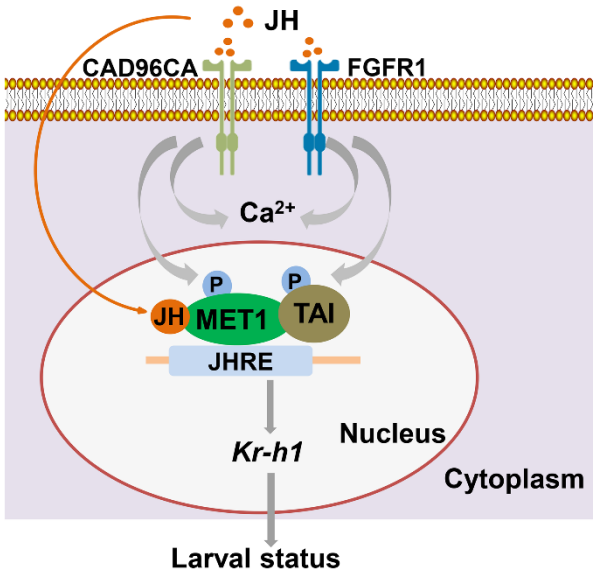

Figure 6. A diagram illustrating CAD96CA and FGFR1 transmit juvenile hormone signal for gene expression. CAD96CA and FGFR1 play roles in JH-induced calcium increase, phosphorylation of MET1 and TAI, and *Kr-h1* expression to maintain larval status. CAD96CA and FGFR1 have high affinity to JH III. JH III transmits the signal by cell membrane receptor CAD96CA and FGFR1 to induce rapid Ca^{2+} signaling, which regulates the phosphorylation of MET and TAI to enhance the function of MET for gene transcription. On the other hand, JH enters cells freely via diffusion to bind its intracellular receptor MET, MET interacts with TAI and then binds to the JH response element (JHRE, containing the E-box core sequence, in the *Kr-h1* promoter region) to promote *Kr-h1* expression to keep larval status. Therefore, JH III transmits signal by either cell membrane receptor and intracellular receptor at different stages in the signaling.

Figure supplement

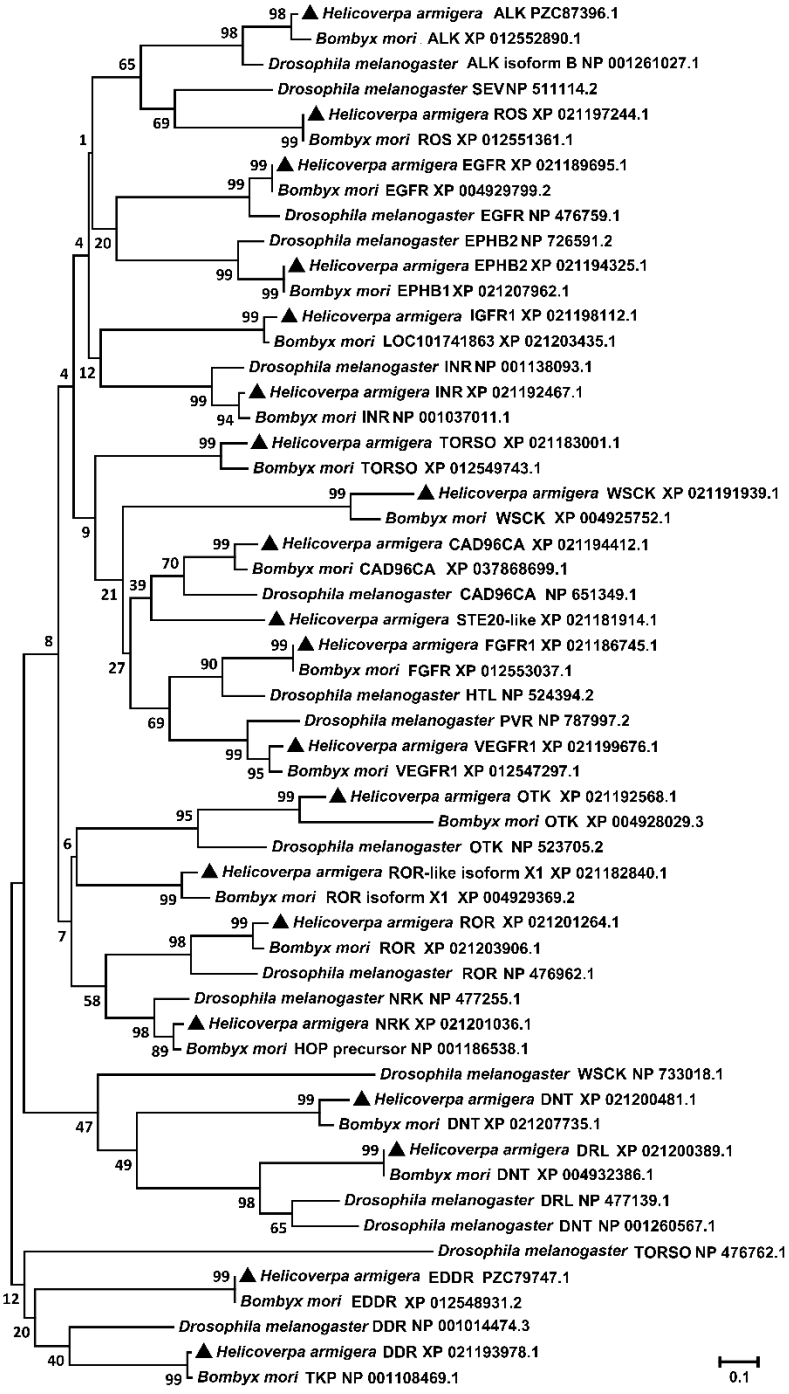

Figure 1—figure supplement 1. Phylogenetic tree analysis to identify RTKs of *H. armigera*. The phylogenetic tree was analyzed with MEGA 5.0, Corresponding amino acid sequences in RTKs of *H. armigera*, *B. mori*, and *D. melanogaster* obtained from NCBI. The tree shows clustering and the clades of various RTK in *H. armigera*, *B. mori*, and *D. melanogaster*. Black triangles represent RTKs in *H. armigera*. NRK was renamed based on the phylogenetic tree. The other RTKs were named based on the *H. armigera* genome.

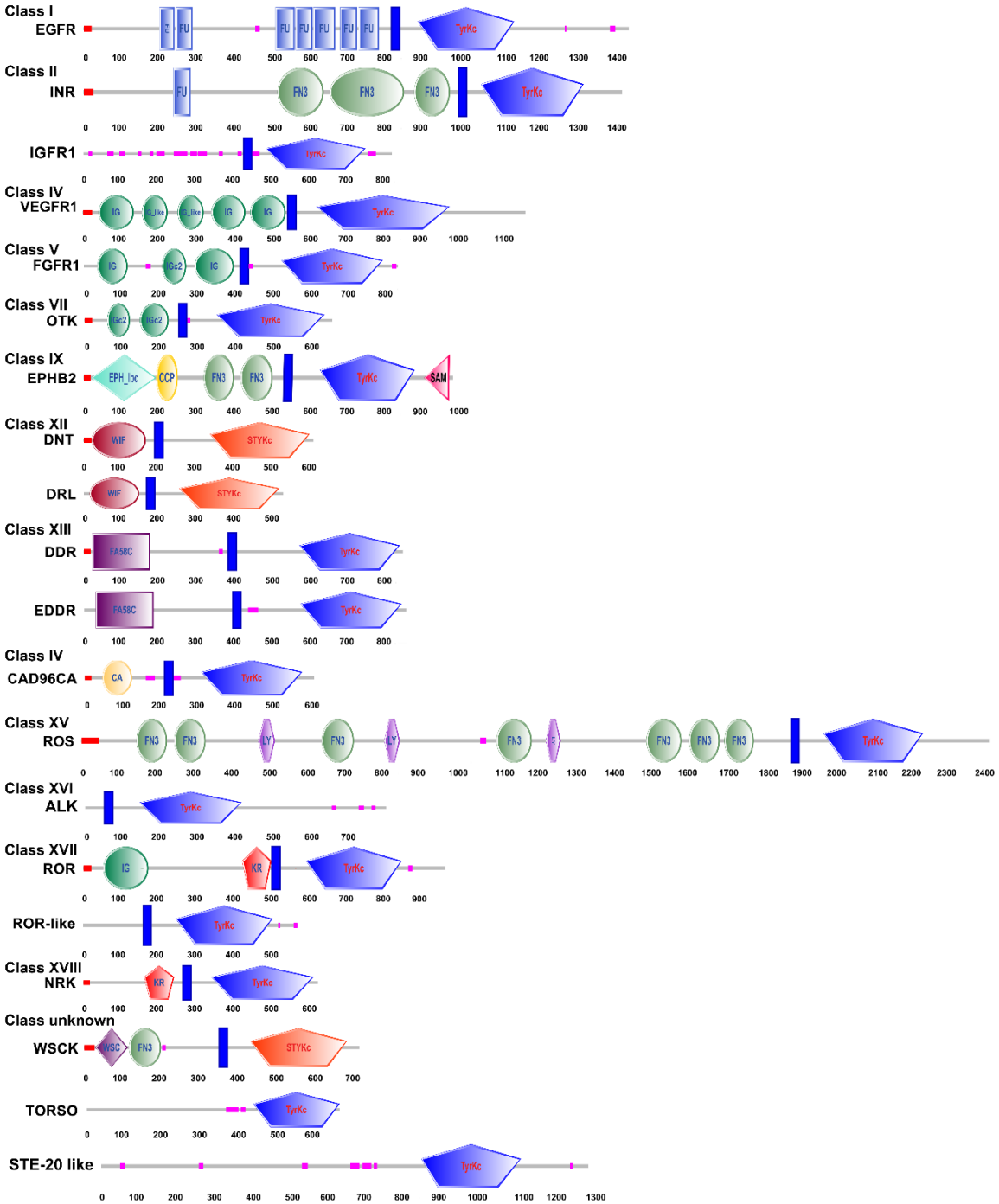

Figure 1—figure supplement 2. Structural characteristics of the RTK domains. The SMART tool was used to analyze the RTKs of *H. armigera.*

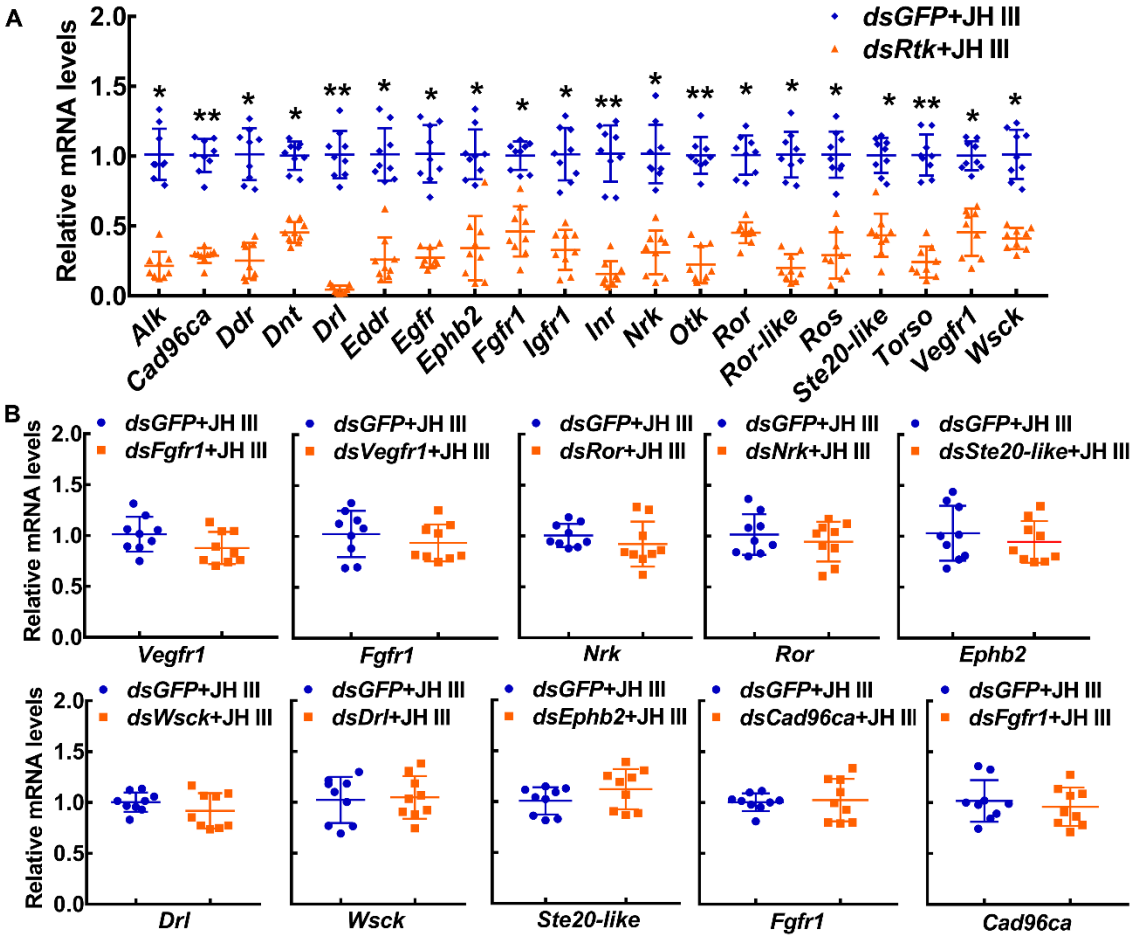

Figure 1—figure supplement 3. The interference efficiency of dsRNA and off–target detection. (**A**) The interference efficiency of dsRNA in HaEpi cells. (**B**) The qRT–PCR was performed to analyze the off–target genes. All of the relative mRNA levels were calculated via the $2^{-\Delta\Delta CT}$ method, and the bars indicate the mean ± SD according to three biological replicates and three technical replicates. Asterisks manifest significant differences by Student's *t* test (**p* < 0.05; ***p* < 0.01).

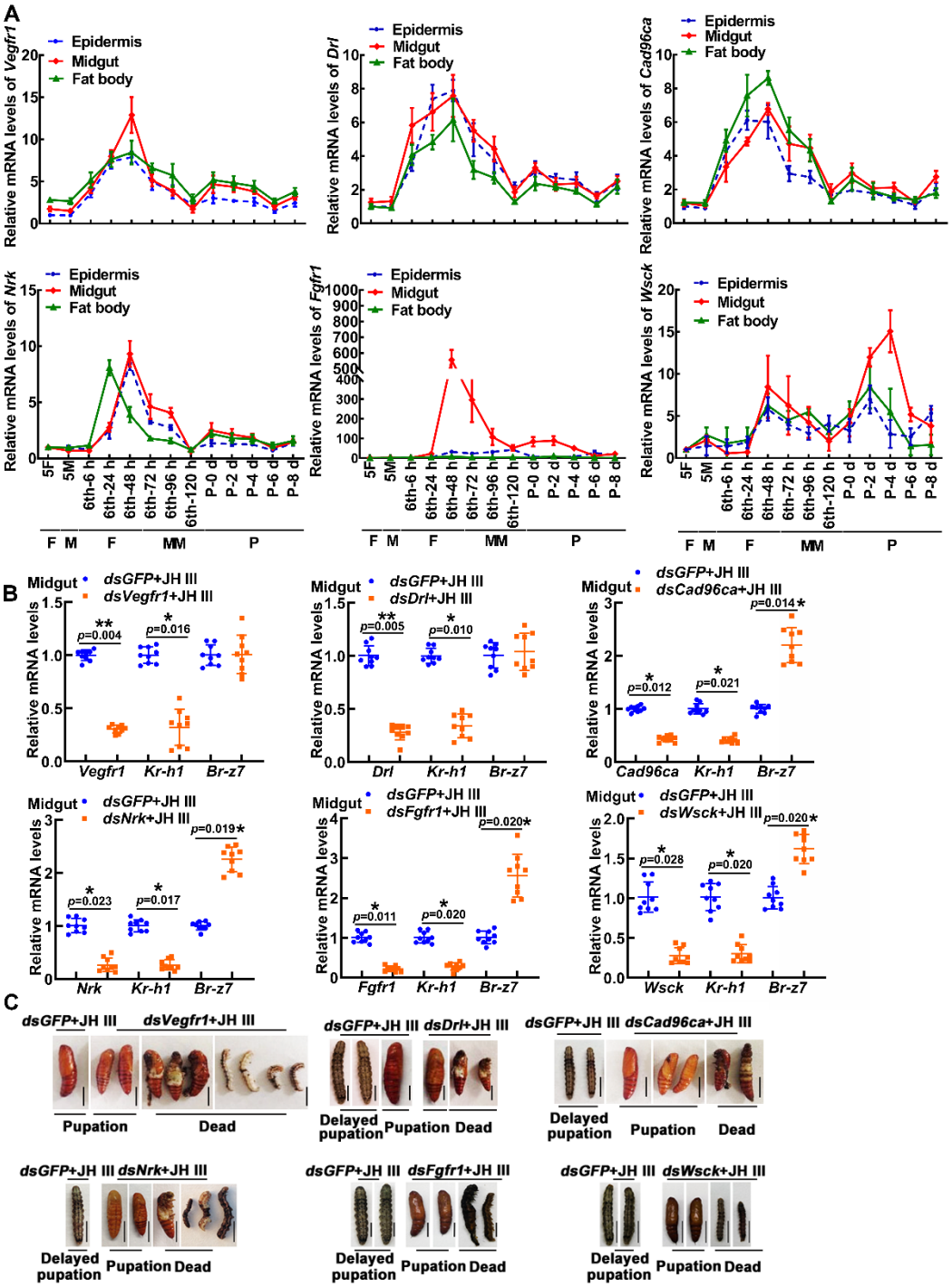

Figure 1—figure supplement 4. Expression profiles, interference efficiency and phenotype of 6 *Rtks* in larvae. (**A**) The expression profiles of *Vegfr1*, *Drl*, *Cad96ca*, *Nrk*, *Fgfr1*, and *Wsck* during development. (**B**) qRT–PCR showed the interference efficiency of *Vegfr1*, *Drl*, *Cad96ca*, *Nrk*, *Fgfr1*, and *Wsck*, and the mRNA level of *Kr-h1* and *Br-z7*. The relative mRNA levels were calculated via the $2^{-\Delta\Delta CT}$ method, and the bars indicate the mean ± SD. Asterisks manifest significant differences by Student's *t* test (*$p < 0.05$; **$p < 0.01$) based on three biological

replicates, n = 3. (**C**) The phenotype after *Vegfr1*, *Drl*, *Cad96ca*, *Nrk*, *Fgfr1*, and *Wsck* knockdown.

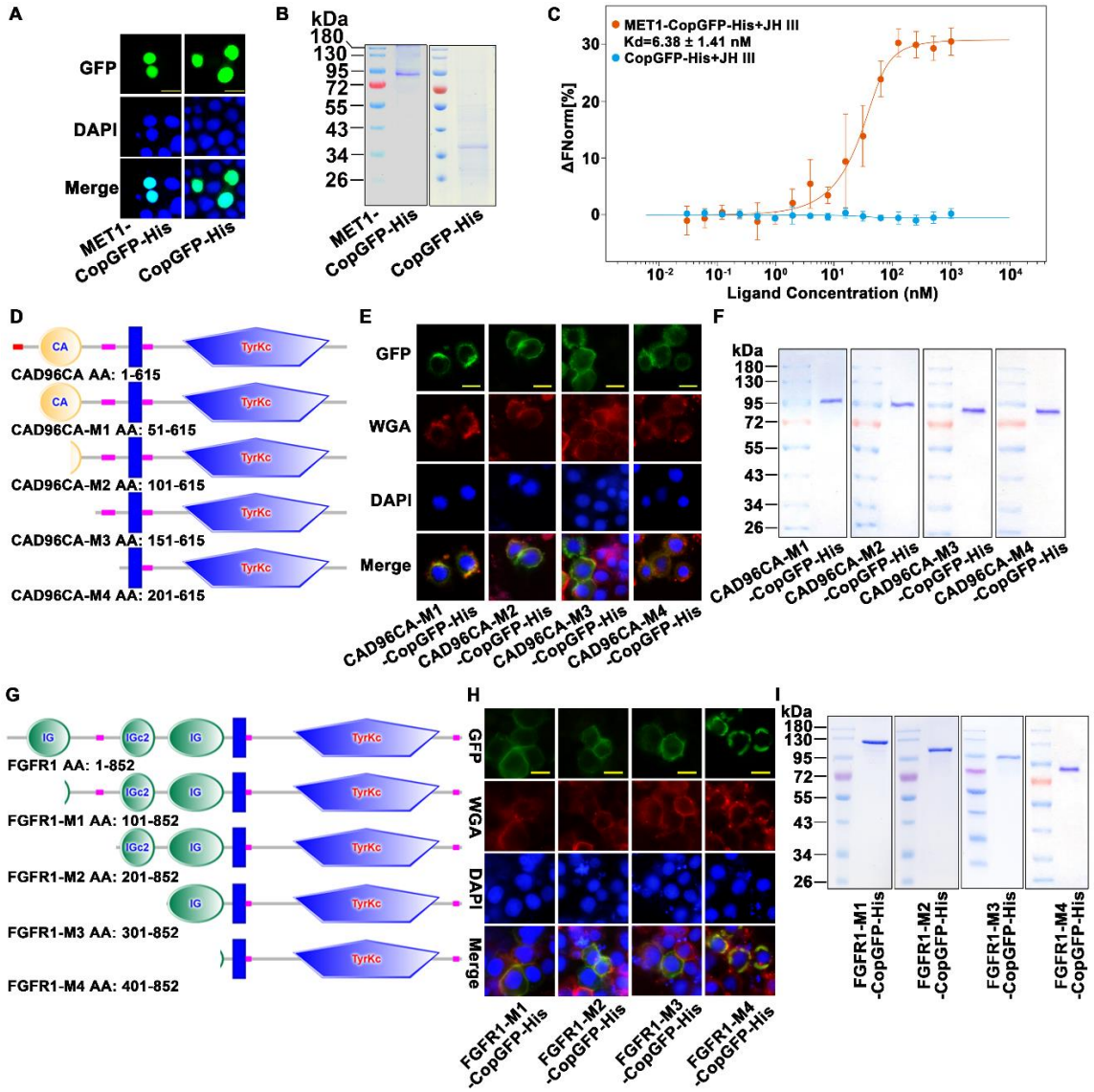

Figure 3—figure supplement 1. MET1 bound JH III, and CAD96CA and FGFR1 mutants. (**A**) The subcellular localization of overexpressed MET1-CopGFP-His and CopGFP-His in the cells. Green: green fluorescence from MET1-CopGFP-His and CopGFP-His. DAPI: nuclear staining. Merge: the pictures of different fluorescence-labelled cells were combined. The cells were observed with a fluorescence microscope. Scale bar=20 μm. (**B**) Coomassie brilliant blue staining of SDS–PAGE gel showing the purity of the separated MET1-CopGFP-His and CopGFP-His proteins. (**C**) Saturation binding curves of MET1-CopGFP-His and CopGFP-His. The error line represents three duplicate SD. (**D**) The diagram of CAD96CA mutation. (**E**) Subcellular localization of the CAD96CA mutants. Green: green fluorescence of mutants fused with a green fluorescent protein. Red: the cell membrane stained with wheat germ lectin (WGA). Blue: nuclei stained with DAPI. Scale = 20 μm. (**F**) Coomassie brilliant blue staining of the SDS–PAGE gel showed the purity of the separated CAD96CA mutant proteins. (**G**) The diagram of FGFR1 mutation. (**H**) Subcellular localization of the FGFR1 mutants. Green: green fluorescence of

mutants fused with a green fluorescent protein. Red: the cell membrane stained with wheat germ lectin (WGA). Blue: nuclei stained with DAPI. Scale = 20 μm. (**I**) Coomassie brilliant blue staining of the SDS–PAGE gel showed the purity of the separated FGFR1 mutant proteins.

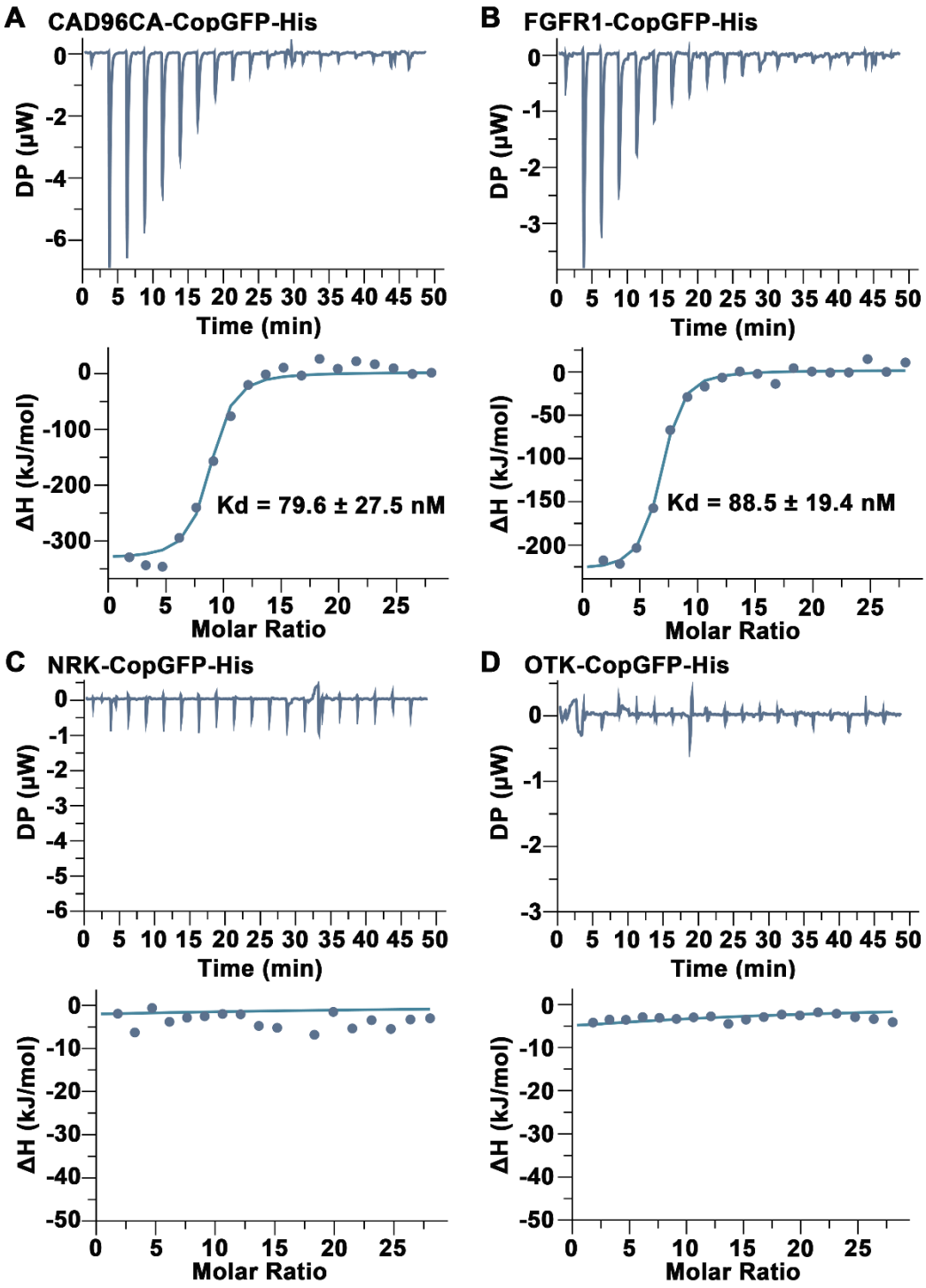

Figure 3—figure supplement 2. CAD96CA and FGFR1 bound JH III were analyzed using ITC. (**A**) Saturation binding curves of CAD96CA-CopGFP-His. (**B**) Saturation binding curves of FGFR1-CopGFP-His. (**C**) The binding curves of NRK-CopGFP-His. (**D**) The binding curves of OTK-CopGFP-His. The data were subtracted with that from the control test by the analysis software.

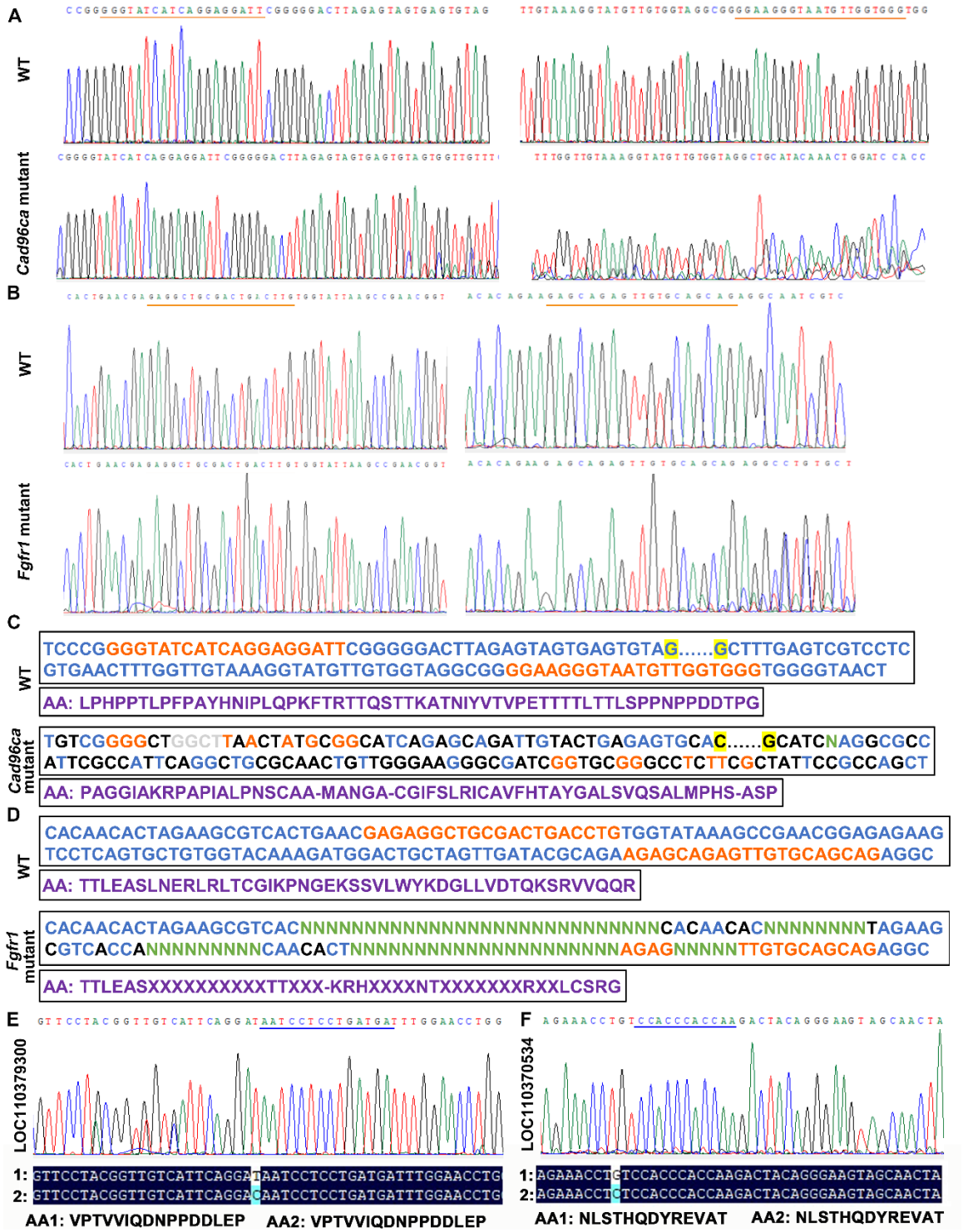

Figure 4—figure supplement 1. Targeted mutagenesis of *Cad96ca* and *Fgfr1* in *H. armigera*. (**A** and **B**) Mutations were detected by Sanger sequencing. Representative chromatograms of the PCR products of G0 *H. armigera* showing mutations induced by the CRISPR/Cas9 system. The gRNA target sequence was marked with an orange line. (**C** and **D**) Examples of G0 mutations identified by TA cloning and Sanger sequencing. The gRNA target sequence was marked in orange. Nucleotide insertions were shown in grey; nucleotide deletions were shown in green (N); and substitutions were shown in black. The purple sequence represents the amino acid sequence. (**E** and **F**) Off–target genes detected by Sanger sequencing. The chromatograms of the PCR products of G0 *H. armigera* showed mutations. The gRNA target sequence was marked with a blue line. 1: mutant sequence, 2: normal sequence.

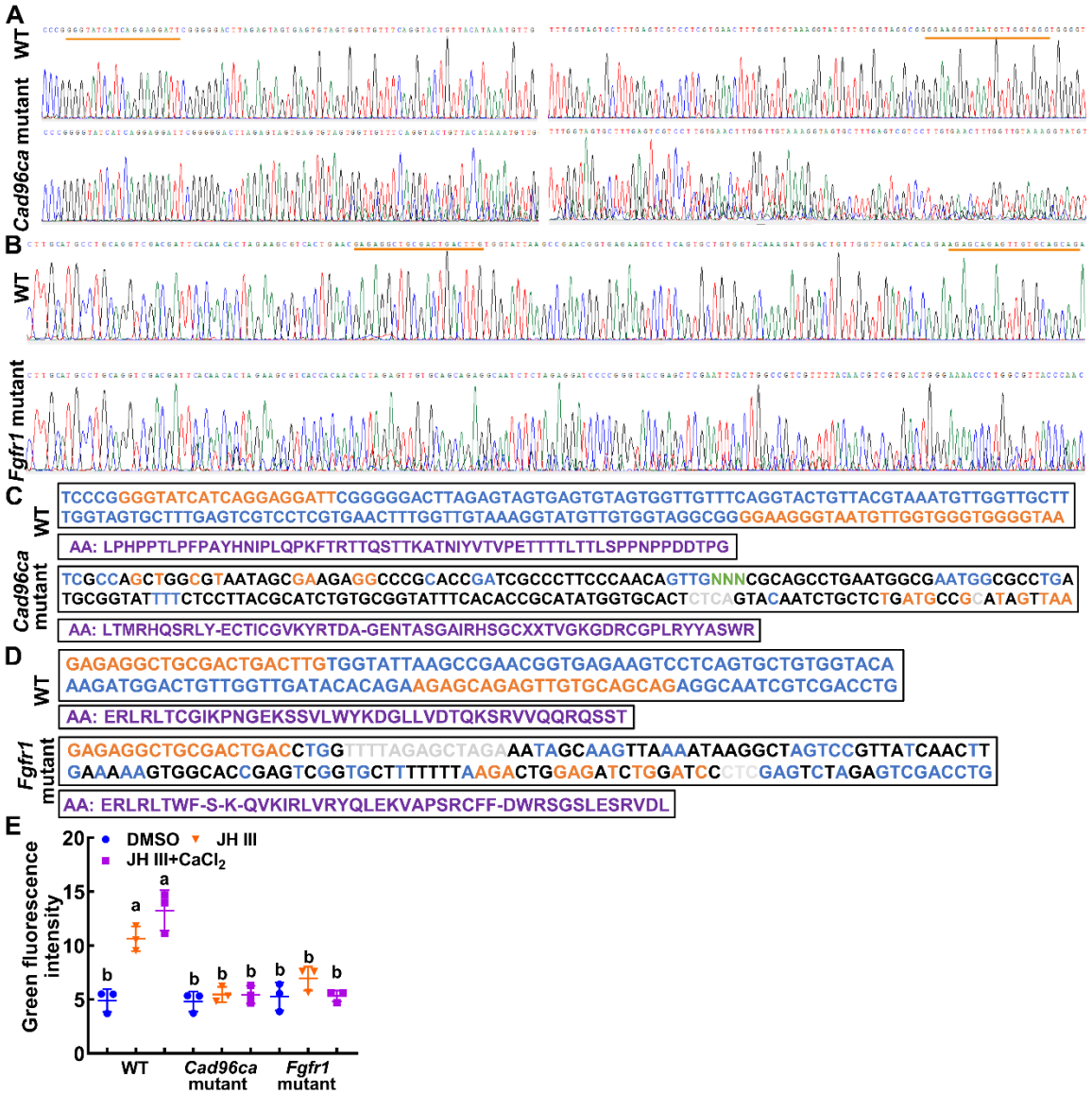

Figure 4—figure supplement 2. Targeted mutagenesis of *Cad96ca* and *Fgfr1* in HaEpi cells. (**A** and **B**) Mutations were detected by Sanger sequencing. Representative chromatograms of the PCR products of mutations. The gRNA target sequence was marked with an orange line. (**C** and **D**) Examples of mutations identified by TA cloning and Sanger sequencing. The gRNA target sequence was marked in orange. Nucleotide insertions were shown in grey, nucleotide deletions

were shown in green (N), and substitutions were shown in black. The purple sequence represents the amino acid sequence. (**E**) Statistical analysis of the green fluorescence signal intensity by ImageJ software. The statistical analysis was performed using three independent replicates by ANOVA.

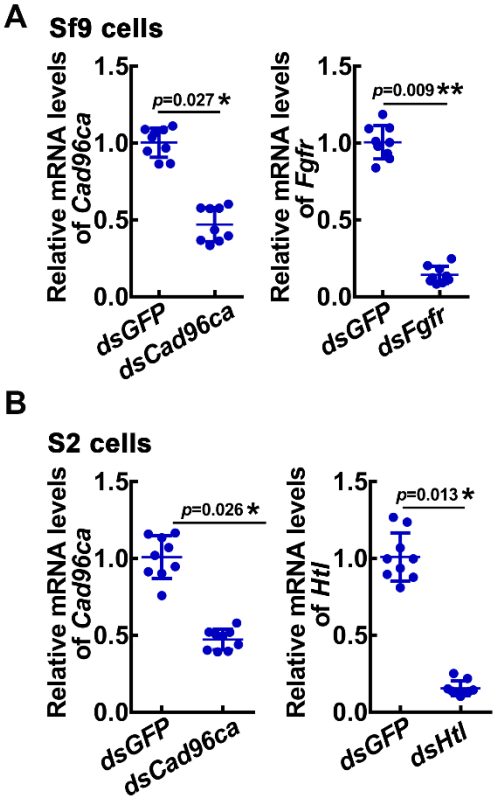

Figure 5—figure supplement 1. The efficiency of the interference experiment was analyzed by qPCR. (**A**) Interference efficiency of *Cad96ca* and *Fgfr* in sf9 cell lines. (**B**) Interference efficiency of *Cad96ca* and *Htr* in S2 cell lines.

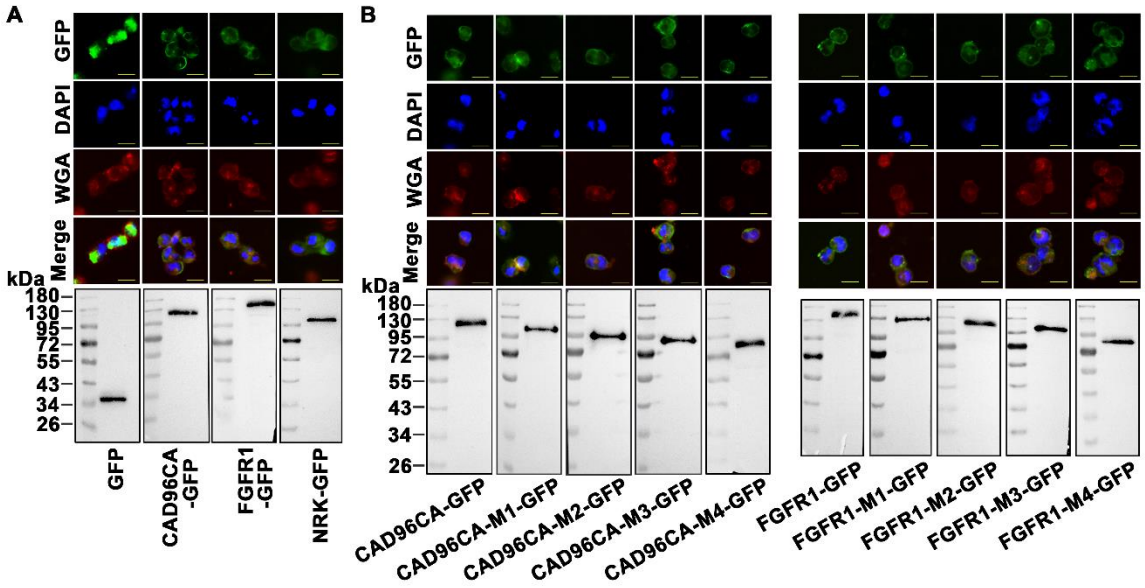

Figure 5—figure supplement 2. CAD96CA, FGFR1 and mutants overexpressed in HEK-293T cells. (**A**) Subcellular localization of overexpressed GFP, CAD96CA-GFP, FGFR1-GFP, and NRK-GFP. GFP: green fluorescence of RTKs fused with a green fluorescent protein. WGA: wheat germ agglutinin, a cell membrane label. DAPI: nuclear staining. Merge: the pictures of different fluorescence-labelled cells were combined. The cells were observed with a fluorescence microscope. Scale bar = 20 μm. Western blotting showed the expression of the target protein. (**B**) Subcellular localization of the CAD96CA and FGFR1 mutants. Green: green fluorescence of mutants fused with a green fluorescent protein. Red: the cell membrane stained with wheat germ lectin (WGA). Blue: nuclei stained with DAPI. Scale = 20 μm. The protein level of the mutant was detected by western blotting.

Supplementary files

Supplementary file 1. Names of RTKs identified in *H. armigera* genome.

Helicoverpa armigera		*Bombyx mori*	*Drosophila melanogaster*
Name	Symbol	Symbol	Symbol
ALK/Anaplastic lymphoma kinase	LOC110383585	ALK	ALK
Cad96Ca/Cadherin 96Ca	LOC110379194	Cad96Ca	Cad96Ca
Ddr/Discoidin domain receptor	LOC110378887	TKP	Ddr
Dnt/Doughnut on	LOC110383864	Dnt isoform X1	Dnt
Drl/Derailed	LOC110383805	Dnt	Drl
EDdr/Epithelial discoidin domain receptor	LOC110374488	EDdr	
EGFR/Epidermal growth factor receptor	LOC110375773	EGFR	Egfr
EphB2/Ephrin type-B receptor 2	LOC110379128	EphB1	EphB2
FGFR1/Fibroblast growth factor receptor homolog 1	LOC110373728	FGFR	Htl/DFR1/Dtk1
IGFR1/Insulin-like growth factor 1 receptor	LOC110381988	LOC101741863	
InR/Insulin-like receptor	LOC110377777	InR	InR
Nrk/Neurotropic receptor kinase	LOC110384207	HOP	Nrk
Otk/Offtrack	LOC110377855	Otk	Otk
Ror/Receptor tyrosine kinase orphan receptor	LOC110384348	Ror	Ror
Ror-like isoform X1/ Receptor tyrosine kinase like orphan receptor	LOC110371076	Ror isoform X1	Ror
ROS/Proto-oncogene tyrosine-protein kinase	LOC110381275	ROS	Sev
STE20-like/serine/ threonine-protein kinase	LOC110370444		

STE20-like			
Torso/tyrosine-protein kinase receptor torso like	LOC110371197	Torso	Torso
VEGFR1/Vascular endothelial growth factor receptor 1	LOC110383235	VEGFR1	Pvr
Wsck/Cell wall integrity and stress response component kinase	LOC110377380	Wsck	Wsck

1114
1115

1116 Supplementary file 2. Oligonucleotide sequences of PCR primers.

Primer name	5´⟶3´ nucleotide sequence
qRT-PCR	
Kr-h1-RTF	atgtttacgagatttcggttac
Kr-h1-RTR	atgtgggcttccatttgtttt
Jhi-1-RTF	accacatcttcatcacaacca
Jhi-1-RTR	tacaactcatccaagccctca
Jhi-26-RTF	gcggatacgaaccacat
Jhi-26-RTR	ggctccactgacacgat
Vg-RTF	gtcaatgaggatgaacaggga
Vg-RTR	gttggcgttagacacgagagg
Torso-RTF	cgggcagataagcacaactc
Torso-RTR	gaggaaaggctcgtttgatg
Otk-RTF	gtgcgtgattcgttcgtt
Otk-RTR	ccttctactcgacttgtggg
Ddr-RTF	gtgtccgaggtcgcaaat
Ddr-RTR	cgataacatacgcctctgc
Wsck-RTF	gattggagtggtggcagtt
Wsck-RTR	tgtggttgccaagggtat
Egfr-RTF	gactatctgatgccctcaccgc
Egfr-RTR	aaccgcaaatcctttattccct
Ste20-like-RTF	ctcgccacgctactccaca
Ste20-like -RTR	tcatactccgccgacagg
Vegfr1-RTF	ttaggttgaaagattacccacg
Vegfr1-RTR	atctccagtacgctcgtgtc
Ror-like-RTF	tcacgcacgaatcagacg
Ror-like-RTR	tggcggcacaagcacta
Fgfr1-RTF	gtggcaacggcgtgtctt
Fgfr1-RTR	aactctgctcttctgcgtatca
Ros-RTF	tcccgctcgtgagtatga
Ros-RTR	tgattgagtgttccgtgctat
Igfr1-RTF	tgctgctgtgcctgctggtg
Igfr1-RTR	cggtgccgagtttccgatta
Inr-RTF	tcttggtacaccgtgaacatc
Inr-RTR	actacgaagccgttggggttctgag
Dnt-RTF	cgagaaactaaggctgaaggtg
Dnt-RTR	gccagaggtgatgctccaag
Drl-RTF	agatgcgagggagcaagaagt
Drl-RTR	gctaacacccaggaccgacag
Cad96ca-RTF	ttcaacctacccgccatca
Cad96ca-RTR	tctccaacccataagtcacag
Alk-RTF	aagaaggcggtgatagacgatt
Alk-RTR	tgactgttggacgaggaggac
Nrk-RTF	ggactacagccaagtaaccac

Nrk-RTR	gaggtcttgtatgctgatgagggta
Ror-RTF	acacgccgcaaaggagac
Ror-RTR	ccgttggaagaggagcag
Ephb2-RTF	cagtgctggagacaaccttcg
Ephb2-RTR	tcggctgtttcttatcacattca
Eddr-RTF	atgcgacctgtcaccttccttg
Eddr-RTR	tgccgctttcacttcgttatgg
RNAi	
Fgfr1-RNAiF	gcgtaatacgactcactatagggagcgtcactgaacgagag
Fgfr1-RNAiR	gcgtaatacgactcactatagggaaacgtggagggaaatat
Vegfr1-RNAiF	gcgtaatacgactcactatagggttgcctcacttcagcc
Vegfr1-RNAiR	gcgtaatacgactcactatagggtttcgcactttccacg
Wsck-RNAiF	gcgtaatacgactcactataggg tttctgtgggaatgcg
Wsck-RNAiR	gcgtaatacgactcactataggggctggggtctggagt
Drl-RNAiF	gcgtaatacgactcactatagggagtggacttgccttgtacg
Drl-RNAiR	gcgtaatacgactcactatagggtcagctctgctatcctttgt
Cad96ca-RNAiF	gcgtaatacgactcactatagggtctacgccacagtctccga
Cad96ca-RNAiR	gcgtaatacgactcactatagggcgtctttcttgctatccttc
Ror-RNAiF	gcgtaatacgactcactatagggggcgtgtatttattgttt
Ror-RNAiR	gcgtaatacgactcactatagggggtgccattagtcttatc
Ephb2-RNAiF	gcgtaatacgactcactatagggatacccactggctcctgt
Ephb2-RNAiR	gcgtaatacgactcactatagggcattctcggcgtaaactt
Nrk-RNAiF	gcgtaatacgactcactatagggttatcgtgcttcttctta
Nrk-RNAiR	gcgtaatacgactcactatagggatgttgtggttacttggc
Ste20-like-RNAiF	gcgtaatacgactcactatagggcagaaaagacctacacagc
Ste20-like-RNAiR	gcgtaatacgactcactatagggcaggcaagtaacgtcacaac
Overexpression	
Nrk-oveF	gattctagagctagcgaattcgccaccatggacattcactttaa
Nrk-oveR	tcgtcgctctccatagcggccgcttcaggatgagttctttccaatatca
Otk-oveF	gattctagagctagcgaattcgccaccatggtgatgtgcgtgattcgttcgttc
Otk-oveR	tcgtcgctctccatagcggccgcctcttcgactttctcctgagatttc
Cad96ca-oveF	gattctagagctagcgaattcgccaccatggtgatgtttctgacaagc
Cad96ca-oveR	tcgtcgctctccatagcggccgctagtttttctccatccaagtgctg
Fgfr1-oveF	gattctagagctagcgaattcgccaccatgaatctcgccg
Fgfr1-oveR	tcgtcgctctccatagcggccgctttgatgaaaggaaagtcactgtca
Mutant	
Cad96ca-M1-F	gattctagagctagcgaattcgccaccatggtgagggtgtaccgtgaag
Cad96ca-M1-R	tcgtcgctctccatagcggccgctagtttttctccatccaagtgctg
Cad96ca-M2-F	gattctagagctagcgaattcgccaccatggtgtgggtgacagcatacg
Cad96ca-M2-R	tcgtcgctctccatagcggccgctagtttttctccatccaagtgctg
Cad96ca-M3-F	gattctagagctagcgaattcgccaccatggtgaggacgactcaaagca
Cad96ca-M3-R	tcgtcgctctccatagcggccgctagtttttctccatccaagtgctg
Cad96ca-M4-F	gattctagagctagcgaattcgccaccatggtgacagaagctcctaata

Cad96ca-M4-R	tcgtcgctctccatagcggccgctagtttttctccatccaagtgctg
Fgfr1-M1-F	gattctagagctagcgaattcgccacctgtaagactgataat
Fgfr1-M1-R	tcgtcgctctccatagcggccgctttgatgaaaggaaagtcactgtca
Fgfr1-M2-F	gattctagagctagcgaattcgccacccaccctacaaaacttt
Fgfr1-M2-R	tcgtcgctctccatagcggccgctttgatgaaaggaaagtcactgtca
Fgfr1-M3-F	gattctagagctagcgaattcgccaccgctgaaaacttgaccg
Fgfr1-M3-R	tcgtcgctctccatagcggccgctttgatgaaaggaaagtcactgtca
Fgfr1-M4-F	gattctagagctagcgaattcgccaccggatacttgactgtat
Fgfr1-M4-R	tcgtcgctctccatagcggccgctttgatgaaaggaaagtcactgtca
Crispr-Cas9 mutant	
Universal primer	aaaagcaccgactcggtgccacttttcaagttgataacggactagccttattttaacttgctattt ctagctctaaaac
Cad96ca-gRNA1	taatacgactcactataggaagggtaatgttggtggggttttagagctagaa
Cad96ca-gRNA2	taatacgactcactatagggtatcatcaggaggattgttttagagctagaa
Cad96ca-gRNAF1	aagtggaagggtaatgttggtggggt
Cad96ca-gRNAR1	taaaaccccaccaacattacccttcc
Cad96ca-gRNAF2	aagtgggtatcatcaggaggattgt
Cad96ca-gRNAR2	taaaacaatcctcctgatgataccc
Cad96ca-testF	gacagaagtctacgccaca
Cad96ca-testR	gcatacaaacaggatcaca
Fgfr1-gRNA1	taatacgactcactatagggaggctgcgactgacctggttttagagctagaa
Fgfr1-gRNA2	taatacgactcactataggagcagagttgtgcagcaggttttagagctagaa
Fgfr1-gRNAF1	aagtgagaggctgcgactgacctggt
Fgfr1-gRNAR1	taaaaccaggtcagtcgcagcctctc
Fgfr1-gRNAF2	aagtagagcagagttgtgcagcaggt
Fgfr1-gRNAR2	taaaacctgctgcacaactctgctct
Fgfr1-testF	acccaataaacaacctca
Fgfr1-testR	ctggtccttctactatacttac
gRNAwf-F	tgattacgaattcccgggaggttatgtagtacacattg
gRNAwf-R	gtgttttacgcgcccgggaaaaaaagcaccgactcggt
*p*Kr-h1F	ccatgattacgaattcccgggcttcgacaattcaaatgtaagtcca
*p*Kr-h1R	tttggcgtcttccatgagctccaccatggtggcgttattcaatgatgatgat
HEK-239T	
Overexpression	
Cad96ca-W-F	ctcgagaccatggtggaattcatgtttctgacaagcgtctggg
Cad96ca-W-R	ctcgcccttgctcatggtacctagtttttctccatccaagtgctg
Cad96ca-M1-F	ctcgagaccatggtggaattcagggtgtaccgtgaaggcagt
Cad96ca-M1-R	ctcgcccttgctcatggtacctagtttttctccatccaagtgctg
Cad96ca-M2-F	ctcgagaccatggtggaattctgggtgacagcatacgacggc
Cad96ca-M2-R	ctcgcccttgctcatggtacctagtttttctccatccaagtgctg
Cad96ca-M3-F	ctcgagaccatggtggaattcaggacgactcaaagcactacc
Cad96ca-M3-R	ctcgcccttgctcatggtacctagtttttctccatccaagtgctg
Cad96ca-M4-F	ctcgagaccatggtggaattcacagaagctcctaataagaat
Cad96ca-M4-R	ctcgcccttgctcatggtacctagtttttctccatccaagtgctg
Fgfr1-W-F	ctcgagaccatggtggaattcatgaatctcgccgccattg
Fgfr1-W-R	ctcgcccttgctcatggtacctttgatgaaaggaaagtcactgtca
Fgfr1-M1-F	ctcgagaccatggtggaattctgtaagactgataatgataatg
Fgfr1-M1-R	ctcgcccttgctcatggtacctttgatgaaaggaaagtcactgtca
Fgfr1-M2-F	ctcgagaccatggtggaattccaccctacaaaactttacaaaat
Fgfr1-M2-R	ctcgcccttgctcatggtacctttgatgaaaggaaagtcactgtca
Fgfr1-M3-F	ctcgagaccatggtggaattcgctgaaaacttgaccgttgtag

Fgfr1-M3-R	ctcgcccttgctcatggtacctttgatgaaaggaaagtcactgtca
Fgfr1-M4-F	ctcgagaccatggtggaattcggatacttgactgtattggaat
Fgfr1-M4-R	ctcgcccttgctcatggtacctttgatgaaaggaaagtcactgtca

1117